Hindawi
Mathematical Problems in Engineering
Volume 2019, Article ID 8573241, 18 pages
https://doi.org/10.1155/2019/8573241

Research Article

Thermoelastic Coupling Vibration and Stability Analysis of Rotating Annular Sector Plates

Yongqiang Yang[1,2] and Zhongmin Wang[3]

[1]*School of Mechanical and Precision Instrument Engineering, Xi'an University of Technology, No. 5 South Jinhua Road, 710048, Xi'an, China*
[2]*College of Mechanical & Electrical Engineering, Shaanxi University of Science & Technology, No. 6 Xuefu Middle Road, 710021, Xi'an, China*
[3]*School of Civil Engineering and Architecture, Xi'an University of Technology, No. 5 South Jinhua Road, 710048 Xi'an, China*

Correspondence should be addressed to Zhongmin Wang; wangzhongm@xaut.edu.cn

Received 1 November 2018; Revised 6 January 2019; Accepted 24 January 2019; Published 5 March 2019

Academic Editor: Francesco Tornabene

This study investigates the thermoelastic coupling vibration and stability of rotating annular sector plates. Based on Hamilton's principle and thermal conduction equation with deformation effect, the differential equation of transverse vibration for a rotating annular sector plate is established. The differential equation of vibration and corresponding boundary conditions are discretized by the differential quadrature method. Then, the thermoelastic coupling transverse vibrations under three different boundary conditions are calculated. The change curve of the first three order dimensionless complex frequencies of the rotating annular sector plate with the dimensionless angular speed are analyzed in the case of the thermoelastic coupling and uncoupling. The effects of the dimensionless angular speed, the ratio of inner to outer radius, the sector angle, and the dimensionless thermoelastic coupling coefficient on transverse vibration and stability of the annular sector plate are discussed. Finally, we obtained the type of instability and corresponding critical speed of the rotating annular sector plate in the case of the thermoelastic coupling and uncoupling.

1. Introduction

As a basic structure, the annular sector plate has been widely used in practical engineering, such as missiles, ships, instruments, and machine structures. The behavior of annular sector plate is very important for these structures, which has attracted great attention from many researchers. Some research work has been done on the bending behavior of the annular sector plate. For example, Jomehzadeh et al. and Sahraee [1, 2] analyzed the bending of functionally graded annular sector plates based on the Levinson plate theory and the first order shear deformation plate theory. Fallah and Nosier [3] reformulated the governing equations of the first order theory into the interior and edge-zone problems of the circular sector plate and analyzed the bending of functionally graded circular sector plates subjected to transverse loading. Qian and Yan [4] studied the bending problems of thin elastic annular sector plate with simply supported along radial edges and free along circular edges by a solution of deflection in the form of Fourier-Bessel double series.

Recently, more and more researchers have realized the importance of vibration analysis of the annular sector plate and have done considerable researches on this topic. On the one hand, some researchers have been devoted to unifying the vibration modeling of circular, annular, and sector plates. For example, Shi et al. and Wang et al. [5–7] established a unified vibration model of circular, annular, and sector plates with arbitrary boundary conditions and presented a unified method based on a new form of trigonometric series expansion for free vibration analysis of circular/annular sector plates. Later, Zhong et al. and Guan et al. [8, 9] applied the models and methods presented above to analyze free vibration of sector-like thin plate with various boundary conditions. Zhao et al. [10] constructed the unified theoretical model of functionally graded porous (FGP) circular, annular, and sector plates with general elastic restraints based on the

first order shear deformation theory and studied free vibration and force vibration of FGP plates. On the other hand, some researchers have studied the effects of the structure and boundary condition on free vibration of the annular sector plate. Rezaei and Saidi [11] studied free vibration response of the fluid-saturated porous annular sector plates by building relative motion model between fluid and solid skeleton of the porous medium. By applying the Ritz method, Zhou et al. [12] obtained natural frequencies of free vibration of annular sector plates based on the three-dimensional elasticity theory. Belalia and Houmat [13] analyzed the nonlinear free vibration of moderately thick functionally graded sector plates by the p-version of the finite element method. Mizusawa [14] investigated free vibration of isotropic annular sector plates with arbitrary boundary conditions by using the spline element method. However, some sector plates rotate at the certain angular speed in many fields of engineering, such as sector mechanism in vibration mill and sector gear in high-speed rapier loom. The researches mentioned above have not involved the effect of the rotating angular speed on vibration characteristics of the annular sector plate.

Furthermore, the annular sector plate is under varying temperature environment in actual engineering applications, which needs to be considered. Behzad et al. [15] used 3D elasticity theory to analyze the thermal buckling of functionally graded perforated annular sector plates. Shaterzadeh et al. [16] used the finite element method to discuss the stability of composite perforated annular sector plates under thermo-mechanical loading. Mirtalaie [17] studied free vibration of functionally graded sector plates in thermal environment and examined the effects of temperature field, volume fraction exponent, radius ratio, and sector angle on free vibrations of the sector plate. The above researches have not involved the interaction between temperature field and strain field. In fact, the temperature field and the strain filed can affect each other, so the thermoelastic coupling should be taken into account in the vibration characteristic analysis of the rotating annular sector plate.

The differential equation of thermoelastic coupling transverse vibration of the rotating annular sector plate is the fourth-order partial differential equation with variable coefficients. The high-order partial differential equation has been solved by the finite element method and Galerkin method in some literature [13, 16, 18–20]. The differential quadrature method (DQM) was firstly proposed by Bellman and Casti in early 1970s [21]. Later, some researchers continued to improve this method and applied it to numerical solution of problems in engineering [22–25]. In recent years, as a numerically accurate and computationally efficient technique, the differential quadrature method (DQM) has also been applied in vibration analysis. Tornabene et al. [26, 27] used the generalized differential quadrature method to study free vibration of functionally graded conical, cylindrical shells and annular plates, and they compared numerical solutions using the DQM with those obtained using commercial programs which show the DQM can provide accurate and computationally efficient results. Fantuzzi [28] used the DQM to analyze free vibration analysis of arbitrarily shaped functionally graded carbon nanotube-reinforced plates. Shao et al. [29] discretized the transverse vibration differential equations of moving membrane by using the DQM and investigated the effects of the density coefficient and the tension ratio on transverse vibration characteristics of the membrane. However, few papers have focused on the fourth-order partial differential equation of thermoelastic coupling transverse vibration by DQM. In this paper, we use the DQM to solve the differential equation of thermoelastic coupling transverse vibration of the rotating annular sector plate.

This study aims to construct the differential equation of thermoelastic coupling transverse vibration of the rotating annular sector plate based on Hamilton's principle and the thermal conduction equation. The dimensionless complex frequencies of the rotating annular sector plate in the case of the thermoelastic coupling and uncoupling are analyzed by the differential quadrature method. The change curve of the first three order dimensionless complex frequencies of the rotating annular sector plate with the dimensionless angular speed is analyzed under different boundary conditions. The effects of the ratio of inner to outer radius, the sector angle, and the dimensionless thermoelastic coupling coefficient on dynamic stability of the rotating annular sector plate are analyzed.

2. Differential Equation of Thermoelastic Coupling Vibration

2.1. Differential Equation of Transverse Vibration with Varying Temperature. Figure 1 shows an annular sector plate with inner radius a, outer radius b, sector angle ϕ, and thickness h. The annular sector plate in the polar coordinate (r, θ) is rotating around an axis perpendicular to its surface with a constant rotating annular speed Ω.

The strain-displacement relation in the middle surface of the rotating annular sector plate can be given by

$$\begin{aligned} \varepsilon_r^0 &= \frac{\partial u}{\partial r} \\ \varepsilon_\theta^0 &= \frac{1}{r}\left(u + \frac{\partial v}{\partial \theta}\right) \\ \gamma_{r\theta}^0 &= \frac{1}{r}\left(\frac{\partial u}{\partial \theta} - v\right) + \frac{\partial v}{\partial r} \end{aligned} \tag{1}$$

where u and v are the displacement field components along the radial direction r and the circumferential direction θ in the middle plane of the rotating annular sector plate, respectively.

The stresses in the middle surface can be written as

$$\begin{aligned} \sigma_r^0 &= \frac{E}{1-\mu^2}\left(\varepsilon_r^0 + \mu\varepsilon_\theta^0\right) \\ &= \frac{E}{1-\mu^2}\left[\frac{\partial u}{\partial r} + \frac{\mu}{r}\left(u + \frac{\partial v}{\partial \theta}\right)\right] \\ \sigma_\theta^0 &= \frac{E}{1-\mu^2}\left(\varepsilon_\theta^0 + \mu\varepsilon_r^0\right) \end{aligned}$$

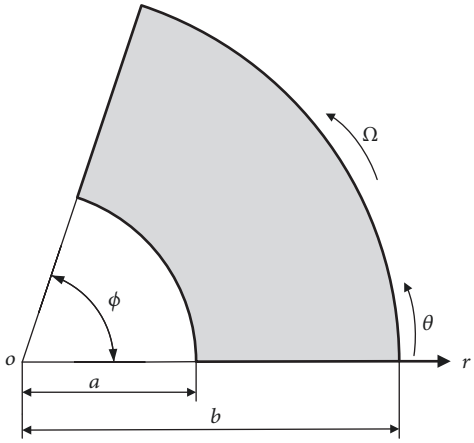

Figure 1: Schematic diagram of the rotating annular sector plate.

$$= \frac{E}{1-\mu^2}\left[\frac{1}{r}\left(u+\frac{\partial v}{\partial \theta}\right)+\mu\frac{\partial u}{\partial r}\right]$$
$$\tau_{r\theta}^0 = \frac{E}{2(1+\mu)}\gamma_{r\theta}^0 = \frac{E}{2(1+\mu)}\left[\frac{1}{r}\left(\frac{\partial u}{\partial \theta}-v\right)+\frac{\partial v}{\partial r}\right] \tag{2}$$

where E is the elastic modulus and μ denotes Poisson's ratio.

The strain-displacement relation at a distance z from the middle surface of the rotating annular sector plate can be given by

$$\varepsilon_r = \frac{\partial u}{\partial r} - z\frac{\partial^2 w}{\partial r^2}$$
$$\varepsilon_\theta = \frac{1}{r}\left(u+\frac{\partial v}{\partial \theta}\right) - z\left(\frac{1}{r}\frac{\partial w}{\partial r}+\frac{1}{r^2}\frac{\partial^2 w}{\partial \theta^2}\right) \tag{3}$$
$$\gamma_{r\theta} = \frac{1}{r}\left(\frac{\partial u}{\partial \theta}-v\right)+\frac{\partial v}{\partial r}-2z\left(\frac{1}{r}\frac{\partial^2 w}{\partial r\partial \theta}-\frac{1}{r^2}\frac{\partial w}{\partial \theta}\right)$$

where w is transverse displacement of the plate.

The corresponding stresses with the varying temperature T can be written as

$$\sigma_r = \frac{E}{1-\mu^2}\left[(\varepsilon_r+\mu\varepsilon_\theta)-(1+\mu)\alpha T\right]$$
$$= \sigma_r^0 - \frac{zE}{1-\mu^2}\left[\frac{\partial^2 w}{\partial r^2}+\mu\left(\frac{1}{r}\frac{\partial w}{\partial r}+\frac{1}{r^2}\frac{\partial^2 w}{\partial \theta^2}\right)\right] - \frac{E\alpha T}{1-\mu}$$
$$\sigma_\theta = \frac{E}{1-\mu^2}\left[(\varepsilon_\theta+\mu\varepsilon_r)-(1+\mu)\alpha T\right] \tag{4}$$
$$= \sigma_\theta^0 - \frac{zE}{1-\mu^2}\left[\left(\frac{1}{r}\frac{\partial w}{\partial r}+\frac{1}{r^2}\frac{\partial^2 w}{\partial \theta^2}\right)+\mu\frac{\partial^2 w}{\partial r^2}\right] - \frac{E\alpha T}{1-\mu}$$
$$\tau_{r\theta} = \frac{E}{2(1+\mu)}\gamma_{r\theta} = \tau_{r\theta}^0 - \frac{zE}{1+\mu}\left(\frac{1}{r}\frac{\partial^2 w}{\partial r\partial \theta}-\frac{1}{r^2}\frac{\partial w}{\partial \theta}\right)$$

where α denotes the linear thermal expansion coefficient.

By using (4), the membrane forces $\{N_r, N_\theta, N_{r\theta}\}$ are given by the following.

$$N_r = \int_{-h/2}^{h/2}\sigma_r dz = h\sigma_r^0$$
$$N_\theta = \int_{-h/2}^{h/2}\sigma_\theta dz = h\sigma_\theta^0 \tag{5}$$
$$N_{r\theta} = \int_{-h/2}^{h/2}\tau_{r\theta} dz = h\tau_{r\theta}^0$$

The bending and twisting moments per unit length are given by

$$M_r = \int_{-h/2}^{h/2}\sigma_r z\, dz$$
$$= -D\left[\frac{\partial^2 w}{\partial r^2}+\mu\left(\frac{1}{r}\frac{\partial w}{\partial r}+\frac{1}{r^2}\frac{\partial^2 w}{\partial \theta^2}\right)\right] - \frac{E\alpha}{1-\mu}M_T$$
$$M_\theta = \int_{-h/2}^{h/2}\sigma_\theta z\, dz \tag{6}$$
$$= -D\left[\left(\frac{1}{r}\frac{\partial w}{\partial r}+\frac{1}{r^2}\frac{\partial^2 w}{\partial \theta^2}\right)+\mu\frac{\partial^2 w}{\partial r^2}\right] - \frac{E\alpha}{1-\mu}M_T$$
$$M_{r\theta} = \int_{-h/2}^{h/2}\tau_{r\theta} z\, dz = -D(1-\mu)\left(\frac{1}{r}\frac{\partial^2 w}{\partial r\partial \theta}-\frac{1}{r^2}\frac{\partial w}{\partial \theta}\right)$$

where $D = Eh^3/12(1-\mu^2)$ is the flexural rigidity and $M_T = \int_{-h/2}^{h/2} Tz dz$ indicates the thermal moment.

The kinetic energy is

$$T = \frac{1}{2}\int_a^b\int_0^\phi \rho h\left(\Omega\frac{\partial w}{\partial \theta}+\frac{\partial w}{\partial t}\right)^2 r dr d\theta \tag{7}$$

and the potential energy is

$$U = \frac{1}{2}\int_a^b\int_0^\phi \left(M_r\kappa_r + M_\theta\kappa_\theta + M_{r\theta}\kappa_{r\theta}\right) r dr d\theta \tag{8}$$

where $\kappa_r = -\partial^2 w/\partial r^2$, $\kappa_\theta = -(1/r)(\partial w/\partial r) - (1/r^2)(\partial^2 w/\partial \theta^2)$, $\kappa_{r\theta} = -(2/r)(\partial^2 w/\partial r\partial \theta) + (2/r^2)(\partial w/\partial \theta)$.

Considering the symmetry of rotation, the strain produced by rotation is a function of r, which is independent of θ, so $N_{r\theta} = 0$. Based on the above analyses, the force balance condition in the axisymmetric annular sector plate is given by

$$\frac{\partial N_r}{\partial r}+\frac{N_r - N_\theta}{r}+q = 0 \tag{9}$$

where $q = \rho h\Omega^2 r$ is the inertial force per unit area in the middle surface and ρ denotes the density of materials.

The strain energy due to the rotating centrifugal force is reduced to the following.

$$V = \frac{1}{2}\int_a^b\int_0^\phi \left[N_r\left(\frac{\partial w}{\partial r}\right)^2 + N_\theta\left(\frac{\partial w}{r\partial \theta}\right)^2\right] r dr d\theta \tag{10}$$

The equation of motion of the rotating annular sector plate can be obtained from the following Hamilton's principle.

$$\int_{t_1}^{t_2} (\delta T - \delta U - \delta V)\, \mathrm{d}t = 0 \tag{11}$$

Substituting (7), (8), and (10) into (11) and using (9), the differential equation of transverse vibration can be obtained.

$$\begin{aligned} D\Bigg(&\frac{\partial^4 w}{\partial r^4} + \frac{2}{r}\frac{\partial^3 w}{\partial r^3} - \frac{1}{r^2}\frac{\partial^2 w}{\partial r^2} - \frac{2}{r^3}\frac{\partial^3 w}{\partial r \partial \theta^2} + \frac{1}{r^3}\frac{\partial w}{\partial r} \\ &+ \frac{2}{r^2}\frac{\partial^4 w}{\partial r^2 \partial \theta^2} + \frac{4}{r^4}\frac{\partial^2 w}{\partial \theta^2} + \frac{1}{r^4}\frac{\partial^4 w}{\partial \theta^4}\Bigg) + \frac{E\alpha}{1-\mu}\Bigg(\frac{\partial^2}{\partial r^2} \\ &+ \frac{1}{r}\frac{\partial}{\partial r} + \frac{1}{r^2}\frac{\partial^2}{\partial \theta^2}\Bigg) M_T + \rho h\Bigg(\frac{\partial^2 w}{\partial t^2} + 2\Omega\frac{\partial^2 w}{\partial t \partial \theta} \\ &+ \Omega^2\frac{\partial^2 w}{\partial \theta^2}\Bigg) - N_r\frac{\partial^2 w}{\partial r^2} - N_\theta\Bigg(\frac{1}{r}\frac{\partial w}{\partial r} + \frac{1}{r^2}\frac{\partial^2 w}{\partial \theta^2}\Bigg) \\ &+ \rho h\Omega^2 r\frac{\partial w}{\partial r} = 0 \end{aligned} \tag{12}$$

Given that the varying temperature T along the lateral direction is considerably larger than that along radial direction, the thermal conduction equation can be described as follows

$$\begin{aligned} &\frac{\partial T}{\partial t} - \frac{k}{\rho C_v}\frac{\partial^2 T}{\partial z^2} \\ &\quad + \frac{E\alpha T_0}{(1-2\mu)\rho C_v}\frac{\partial}{\partial t}\Bigg(-z\frac{\partial^2 w}{\partial r^2} - z\frac{1}{r}\frac{\partial w}{\partial r} - z\frac{1}{r^2}\frac{\partial^2 w}{\partial \theta^2}\Bigg) \\ &= 0 \end{aligned} \tag{13}$$

where $T = T(z,t)$ is the varying temperature, k denotes the thermal conductivity, C_v indicates the specific heat at a constant volume, and T_0 represents the initial temperature of the plate.

Equation (12) involves $T(z,t)$, and (13) involves $w = w(r,t)$. In this way, the temperature and deflection fields are coupled together, and the coupling method must be used to solve both equations.

2.2. Solution of N_r and N_θ. In order to solve (12) and (13), N_r and N_θ need to be solved firstly. Considering the symmetry of rotation, the relationship between strain and displacement in the middle surface is written as follows.

$$\begin{aligned} \varepsilon_r^0 &= \frac{\partial u}{\partial r} \\ \varepsilon_\theta^0 &= \frac{u}{r} \\ \gamma_{r\theta}^0 &= 0 \end{aligned} \tag{14}$$

The membrane forces can be written as follows.

$$\begin{aligned} N_r &= \frac{Eh}{1-\mu^2}\left(\frac{\partial u}{\partial r} + \frac{\mu}{r}u\right) \\ N_\theta &= \frac{Eh}{1-\mu^2}\left(\frac{1}{r}u + \mu\frac{\partial u}{\partial r}\right) \\ N_{r\theta} &= 0 \end{aligned} \tag{15}$$

Based on (14), the strain compatibility equation is obtained.

$$\varepsilon_r^0 = \frac{\partial\left(r\varepsilon_\theta^0\right)}{\partial r} \tag{16}$$

Considering that the varying temperature T along the radial direction r is ignored, the following equation is derived by using (9) and (16).

$$r^2\frac{\partial^2 N_r}{\partial r^2} + 3r\frac{\partial N_r}{\partial r} + (3+\mu)\rho h\Omega^2 r^2 = 0 \tag{17}$$

From (17), the solution of N_r can be obtained.

$$N_r = -\frac{(3+\mu)\rho h\Omega^2 r^2}{8} + A + \frac{B}{r^2} \tag{18}$$

Substituting (18) into (9), N_θ can be obtained

$$N_\theta = -\frac{(1+3\mu)\rho h\Omega^2 r^2}{8} + A - \frac{B}{r^2} \tag{19}$$

where A and B are integral constants.

Based on (15), (18), and (19), one obtains the following.

$$\begin{aligned} u = \frac{r}{Eh}\Bigg[&\frac{\left(-1+\mu^2\right)\rho h\Omega^2 r^2}{8} + (1-\mu)A \\ &+ (-1-\mu)\frac{B}{r^2}\Bigg] \end{aligned} \tag{20}$$

The boundary conditions of clamped or simply supported edge at the inner radius ($r = a$) and outer radius ($r = b$) are given by

$$\begin{aligned} u|_{r=a} &= 0 \\ u|_{r=b} &= 0 \end{aligned} \tag{21}$$

while the boundary conditions of free edge at the inner radius ($r = a$) and outer radius ($r = b$) are as follows.

$$\begin{aligned} \sigma_r^0\big|_{r=a} &= 0 \\ \sigma_r^0\big|_{r=b} &= 0 \end{aligned} \tag{22}$$

Substituting (20) into (21), A and B can be determined by the above boundary conditions, and then, N_r and N_θ of the annular sector plate with the two radial edges having clamped or simply supported can be obtained.

$$N_r = \left(-\frac{(3+\mu) r^2}{8} + \frac{(1+\mu)\left(a^2+b^2\right)}{8} + (1-\mu)\frac{a^2b^2}{8r^2} \right) \rho h \Omega^2$$
$$N_\theta = \left(-\frac{(1+3\mu) r^2}{8} + \frac{(1+\mu)\left(a^2+b^2\right)}{8} - (1-\mu)\frac{a^2b^2}{8r^2} \right) \rho h \Omega^2 \tag{23}$$

Similarly, N_r and N_θ of the annular sector plate with the two free radial edges can be obtained by substituting (18) into (22).

$$N_r = \left(-\frac{(3+\mu)\left(r^2-a^2\right)}{8} + \frac{(3+\mu)\left(r^2-a^2\right)b^2}{8r^2} \right) \cdot \rho h \Omega^2$$
$$N_\theta = \left(-\frac{(1+3\mu) r^2}{8} + \frac{(3+\mu)\left(a^2+b^2\right)}{8} + \frac{(3+\mu) a^2b^2}{8r^2} \right) \rho h \Omega^2 \tag{24}$$

2.3. Dimensionless Differential Equation and Boundary Conditions. The following dimensionless quantities are introduced as follows.

$$\overline{r} = \frac{r}{b},$$
$$\overline{w} = \frac{w}{h},$$
$$\overline{\theta} = \frac{\theta}{\phi},$$
$$\overline{z} = \frac{z}{h},$$
$$\tau = \frac{th}{b^2}\sqrt{\frac{E}{12\rho\left(1-\mu^2\right)}},$$
$$\xi = \frac{a}{b},$$
$$c = \frac{b^2\Omega}{h}\sqrt{\frac{\rho}{E}} \tag{25}$$

As a result, (12) and (13) take the form of

$$\left(\frac{\partial^4 \overline{w}}{\partial \overline{r}^4} + \frac{2}{\overline{r}}\frac{\partial^3 \overline{w}}{\partial \overline{r}^3} - \frac{1}{\overline{r}^2}\frac{\partial^2 \overline{w}}{\partial \overline{r}^2} - \frac{2}{\overline{r}^3\phi^2}\frac{\partial^3 \overline{w}}{\partial \overline{r}\partial \overline{\theta}^2} + \frac{1}{\overline{r}^3}\frac{\partial \overline{w}}{\partial \overline{r}} + \frac{2}{\overline{r}^2\phi^2}\frac{\partial^4 \overline{w}}{\partial \overline{r}^2\partial \overline{\theta}^2} + \frac{4}{\overline{r}^4\phi^2}\frac{\partial^2 \overline{w}}{\partial \overline{\theta}^2} + \frac{1}{\overline{r}^4\phi^4}\frac{\partial^4 \overline{w}}{\partial \overline{\theta}^4} \right) + A_1\left(\frac{\partial^2 \overline{M}_T}{\partial \overline{r}^2} + \frac{1}{\overline{r}}\frac{\partial \overline{M}_T}{\partial \overline{r}} + \frac{1}{\overline{r}^2\phi^2}\frac{\partial^2 \overline{M}_T}{\partial \overline{\theta}^2} \right) + \left(\frac{\partial^2 \overline{w}}{\partial \tau^2} + \frac{2\eta^{1/2}c}{\phi}\frac{\partial^2 \overline{w}}{\partial \tau \partial \overline{\theta}} + \frac{\eta c^2}{\phi^2}\frac{\partial^2 \overline{w}}{\partial \overline{\theta}^2} \right) - \eta\left(N_1\frac{\partial^2 \overline{w}}{\partial \overline{r}^2} + N_2\frac{1}{\overline{r}}\frac{\partial \overline{w}}{\partial \overline{r}} + N_2\frac{1}{\overline{r}^2\phi^2}\frac{\partial^2 w}{\partial \overline{\theta}^2} - c^2\overline{r}\frac{\partial \overline{w}}{\partial \overline{r}} \right) = 0 \tag{26}$$

$$\frac{\partial^2 \overline{T}}{\partial \overline{z}^2} - A_2\frac{\partial \overline{T}}{\partial \tau} + A_3\frac{\partial}{\partial \tau}\left(\frac{\partial^2 \overline{w}}{\partial \overline{r}^2} + \frac{1}{\overline{r}}\frac{\partial \overline{w}}{\partial \overline{r}} + \frac{1}{\overline{r}^2\phi^2}\frac{\partial^2 \overline{w}}{\partial \overline{\theta}^2} \right)\overline{z} = 0 \tag{27}$$

where $\overline{M}_T = \int_{-1/2}^{1/2} \overline{T}\overline{z}\,\mathrm{d}\overline{z}$, $\eta = 12(1-\mu^2)$, $A_1 = 12(1+\mu)b^2\alpha T_0/h^2$, $A_2 = (C_v h^3/kb^2)\sqrt{\rho E/12(1-\mu^2)}$, and $A_3 = (E\alpha h^5/(1-2\mu)kb^4)\sqrt{E/12\rho(1-\mu^2)}$.

For simply supported or clamped edge at the inner radius ($\overline{r} = \xi$) and outer radius ($\overline{r} = 1$), N_1 and N_2 are as follows.

$$N_1 = \left(-\frac{(3+\mu)\overline{r}^2}{8} + \frac{1+\mu}{8}\left(1+\xi^2\right) + \frac{1-\mu}{8}\frac{\xi^2}{\overline{r}^2} \right) c^2$$
$$N_2 = \left(-\frac{(1+3\mu)\overline{r}^2}{8} + \frac{1+\mu}{8}\left(1+\xi^2\right) - \frac{1-\mu}{8}\frac{\xi^2}{\overline{r}^2} \right) c^2 \tag{28}$$

For free edges at the inner radius ($\overline{r} = \xi$) and outer radius ($\overline{r} = 1$), N_1 and N_2 are as follows.

$$N_1 = \left(-\frac{(3+\mu)\left(\overline{r}^2-\xi^2\right)}{8} + \frac{(3+\mu)\left(\overline{r}^2-\xi^2\right)}{8\overline{r}^2} \right) c^2$$
$$N_2 = \left(-\frac{(1+3\mu)\overline{r}^2}{8} + \frac{(3+\mu)\left(1+\xi^2\right)}{8} + \frac{(3+\mu)\xi^2}{8\overline{r}^2} \right) c^2 \tag{29}$$

The solution of (26) and (27) is assumed in the following form

$$\overline{w}\left(\overline{r},\overline{\theta},\tau\right) = W\left(\overline{r},\overline{\theta}\right)e^{\mathrm{j}\omega\tau}$$
$$\overline{T}\left(\overline{z},\tau\right) = T^*\left(\overline{z}\right)e^{\mathrm{j}\omega\tau} \tag{30}$$

where $\mathrm{j} = \sqrt{-1}$, τ is the dimensionless time, and ω denotes the dimensionless complex frequency of the rotating annular sector plate.

Substituting (30) into (26) and (27), one obtains the following.

$$\begin{aligned}&\left(\frac{\mathrm{d}^4W}{\mathrm{d}\overline{r}^4}+\frac{2}{\overline{r}}\frac{\mathrm{d}^3W}{\mathrm{d}\overline{r}^3}-\frac{1}{\overline{r}^2}\frac{\mathrm{d}^2W}{\mathrm{d}\overline{r}^2}+\frac{1}{\overline{r}^3}\frac{\mathrm{d}W}{\mathrm{d}\overline{r}}-\frac{2}{\overline{r}^3\phi^2}\frac{\mathrm{d}^3W}{\mathrm{d}\overline{r}\mathrm{d}\overline{\theta}^2}\right.\\&\left.+\frac{2}{\overline{r}^2\phi^2}\frac{\mathrm{d}^4W}{\mathrm{d}\overline{r}^2\mathrm{d}\overline{\theta}^2}+\frac{4}{\overline{r}^4\phi^2}\frac{\mathrm{d}^2W}{\mathrm{d}\overline{\theta}^2}+\frac{1}{\overline{r}^4\phi^4}\frac{\mathrm{d}^4W}{\mathrm{d}\overline{\theta}^4}\right)\\&+A_1\left(\frac{\mathrm{d}^2}{\mathrm{d}\overline{r}^2}+\frac{1}{\overline{r}}\frac{\mathrm{d}}{\mathrm{d}\overline{r}}+\frac{1}{\overline{r}^2\phi^2}\frac{\mathrm{d}^2}{\mathrm{d}\overline{\theta}^2}\right)\int_{-1/2}^{1/2}T^*\overline{z}\mathrm{d}\overline{z}\\&+\left(-\omega^2W+\frac{2\mathrm{j}\omega\eta^{1/2}c}{\phi}\frac{\mathrm{d}W}{\mathrm{d}\overline{\theta}}+\frac{\eta c^2}{\phi^2}\frac{\mathrm{d}^2W}{\mathrm{d}\overline{\theta}^2}\right)\\&-\eta\left(N_1\frac{\mathrm{d}^2W}{\mathrm{d}\overline{r}^2}+N_2\frac{1}{\overline{r}}\frac{\mathrm{d}W}{\mathrm{d}\overline{r}}+N_2\frac{1}{\overline{r}^2\phi^2}\frac{\mathrm{d}^2W}{\mathrm{d}\overline{\theta}^2}\right.\\&\left.-c^2\overline{r}\frac{\mathrm{d}W}{\mathrm{d}\overline{r}}\right)=0\end{aligned}\tag{31}$$

$$\begin{aligned}&\frac{\mathrm{d}^2T^*}{\mathrm{d}\overline{z}^2}-A_2\mathrm{j}\omega T^*+A_3\mathrm{j}\omega\left(\frac{\mathrm{d}^2W}{\mathrm{d}\overline{r}^2}+\frac{1}{\overline{r}}\frac{\mathrm{d}W}{\mathrm{d}\overline{r}}\right.\\&\left.+\frac{1}{\overline{r}^2\phi^2}\frac{\mathrm{d}^2W}{\mathrm{d}\overline{\theta}^2}\right)\overline{z}=0\end{aligned}\tag{32}$$

From (32), the solution of T^* can be obtained

$$\begin{aligned}T^*&=a_1e^{\zeta\overline{z}}+a_2e^{-\zeta\overline{z}}\\&+\frac{E\alpha h^2}{(1-2\mu)\rho C_v b^2}\left(\frac{\mathrm{d}^2W}{\mathrm{d}\overline{r}^2}+\frac{1}{\overline{r}}\frac{\mathrm{d}W}{\mathrm{d}\overline{r}}+\frac{1}{\overline{r}^2\phi^2}\frac{\mathrm{d}^2W}{\mathrm{d}\overline{\theta}^2}\right)\\&\cdot\overline{z}\end{aligned}\tag{33}$$

where a_1 and a_2 are two integral constants and $\zeta=\sqrt{A_2\mathrm{j}\omega}$.

Substituting (33) into (31) results in

$$\begin{aligned}&(1+\psi)\left(\frac{\mathrm{d}^4W}{\mathrm{d}\overline{r}^4}+\frac{2}{\overline{r}}\frac{\mathrm{d}^3W}{\mathrm{d}\overline{r}^3}-\frac{1}{\overline{r}^2}\frac{\mathrm{d}^2W}{\mathrm{d}\overline{r}^2}+\frac{1}{\overline{r}^3}\frac{\mathrm{d}W}{\mathrm{d}\overline{r}}\right.\\&-\frac{2}{\overline{r}^3\phi^2}\frac{\mathrm{d}^3W}{\mathrm{d}\overline{r}\mathrm{d}\overline{\theta}^2}+\frac{2}{\overline{r}^2\phi^2}\frac{\mathrm{d}^4W}{\mathrm{d}\overline{r}^2\mathrm{d}\overline{\theta}^2}+\frac{4}{\overline{r}^4\phi^2}\frac{\mathrm{d}^2W}{\mathrm{d}\overline{\theta}^2}\\&\left.+\frac{1}{\overline{r}^4\phi^4}\frac{\mathrm{d}^4W}{\mathrm{d}\overline{\theta}^4}\right)+\left(-\omega^2W+\frac{2\mathrm{j}\omega\eta^{1/2}c}{\phi}\frac{\mathrm{d}W}{\mathrm{d}\overline{\theta}}\right.\\&\left.+\frac{\eta c^2}{\phi^2}\frac{\mathrm{d}^2W}{\mathrm{d}\overline{\theta}^2}\right)-\eta\left(N_1\frac{\mathrm{d}^2W}{\mathrm{d}\overline{r}^2}+N_2\frac{1}{\overline{r}}\frac{\mathrm{d}W}{\mathrm{d}\overline{r}}\right.\\&\left.+N_2\frac{1}{\overline{r}^2\phi^2}\frac{\mathrm{d}^2W}{\mathrm{d}\overline{\theta}^2}-c^2\overline{r}\frac{\mathrm{d}W}{\mathrm{d}\overline{r}}\right)=0\end{aligned}\tag{34}$$

where $\psi=(1+\mu)E\alpha^2T_0/(1-2\mu)\rho C_v$ is the dimensionless thermoelastic coupling coefficient and indicates the coupling degree between the temperature and strain.

Figures 2(a), 2(b), and 2(c) present the definitions of the boundary conditions. The clamped, simply supported, and free boundary conditions are abbreviated as letters C, S, and F, respectively. For example, the symbolism SS-CC identifies an annular sector plate with the two radial edges having simply supported boundary conditions and the two circular edges having clamped boundary conditions, respectively.

Considering that the edge of plate is held at a constant temperature, the dimensionless boundary conditions of CC-CC, SS-CC, and SS-FF are given as follows, respectively.

$$\text{CC-CC:}\begin{cases}W|_{\overline{r}=\xi}=W|_{\overline{r}=1}=W|_{\overline{\theta}=0}=W|_{\overline{\theta}=1}=0\\\left.\dfrac{\mathrm{d}W}{\mathrm{d}\overline{r}}\right|_{\overline{r}=\xi}=\left.\dfrac{\mathrm{d}W}{\mathrm{d}\overline{r}}\right|_{\overline{r}=1}=\left.\dfrac{\mathrm{d}W}{\mathrm{d}\overline{\theta}}\right|_{\overline{\theta}=0}=\left.\dfrac{\mathrm{d}W}{\mathrm{d}\overline{\theta}}\right|_{\overline{\theta}=1}=0\end{cases}\tag{35}$$

$$\text{SS-CC:}\begin{cases}W|_{\overline{r}=\xi}=W|_{\overline{r}=1}=W|_{\overline{\theta}=0}=W|_{\overline{\theta}=1}=0\\\left.\dfrac{\mathrm{d}W}{\mathrm{d}\overline{r}}\right|_{\overline{r}=\xi}=\left.\dfrac{\mathrm{d}W}{\mathrm{d}\overline{r}}\right|_{\overline{r}=1}=0\\\left.\left(\dfrac{1}{\overline{r}}\dfrac{\mathrm{d}W}{\mathrm{d}\overline{r}}+\dfrac{1}{\overline{r}^2\phi^2}\dfrac{\mathrm{d}^2W}{\mathrm{d}\overline{\theta}^2}+\mu\dfrac{\mathrm{d}^2W}{\mathrm{d}\overline{r}^2}\right)\right|_{\overline{\theta}=0}=\left.\left(\dfrac{1}{\overline{r}}\dfrac{\mathrm{d}W}{\mathrm{d}\overline{r}}+\dfrac{1}{\overline{r}^2\phi^2}\dfrac{\mathrm{d}^2W}{\mathrm{d}\overline{\theta}^2}+\mu\dfrac{\mathrm{d}^2W}{\mathrm{d}\overline{r}^2}\right)\right|_{\overline{\theta}=1}=0\end{cases}\tag{36}$$

$$\text{SS-FF:}\begin{cases}W|_{\overline{\theta}=0}=W|_{\overline{\theta}=1}=0\\\left.\left(\dfrac{1}{\overline{r}}\dfrac{\mathrm{d}W}{\mathrm{d}\overline{r}}+\dfrac{1}{\overline{r}^2\phi^2}\dfrac{\mathrm{d}^2W}{\mathrm{d}\overline{\theta}^2}+\mu\dfrac{\mathrm{d}^2W}{\mathrm{d}\overline{r}^2}\right)\right|_{\overline{\theta}=0}=\left.\left(\dfrac{1}{\overline{r}}\dfrac{\mathrm{d}W}{\mathrm{d}\overline{r}}+\dfrac{1}{\overline{r}^2\phi^2}\dfrac{\mathrm{d}^2W}{\mathrm{d}\overline{\theta}^2}+\mu\dfrac{\mathrm{d}^2W}{\mathrm{d}\overline{r}^2}\right)\right|_{\overline{\theta}=1}=0\\\left.\left(\dfrac{\mathrm{d}^2W}{\mathrm{d}\overline{r}^2}+\mu\dfrac{1}{\overline{r}}\dfrac{\mathrm{d}W}{\mathrm{d}\overline{r}}+\mu\dfrac{1}{\overline{r}^2\phi^2}\dfrac{\mathrm{d}^2W}{\mathrm{d}\overline{\theta}^2}\right)\right|_{\overline{r}=\xi}=\left.\left(\dfrac{\mathrm{d}^2W}{\mathrm{d}\overline{r}^2}+\mu\dfrac{1}{\overline{r}}\dfrac{\mathrm{d}W}{\mathrm{d}\overline{r}}+\mu\dfrac{1}{\overline{r}^2\phi^2}\dfrac{\mathrm{d}^2W}{\mathrm{d}\overline{\theta}^2}\right)\right|_{\overline{r}=1}=0\\\left.\left(\dfrac{\mathrm{d}^3W}{\mathrm{d}\overline{r}^3}+\dfrac{1}{\overline{r}}\dfrac{\mathrm{d}^2W}{\mathrm{d}\overline{r}^2}-\dfrac{1}{\overline{r}^2}\dfrac{\mathrm{d}W}{\mathrm{d}\overline{r}}+\dfrac{2-\mu}{\overline{r}^2\phi^2}\dfrac{\mathrm{d}^3W}{\mathrm{d}\overline{r}\mathrm{d}\overline{\theta}^2}-\dfrac{3-\mu}{\overline{r}^3\phi^2}\dfrac{\mathrm{d}^2W}{\mathrm{d}\overline{\theta}^2}\right)\right|_{\overline{r}=\xi}=\left.\left(\dfrac{\mathrm{d}^3W}{\mathrm{d}\overline{r}^3}+\dfrac{1}{\overline{r}}\dfrac{\mathrm{d}^2W}{\mathrm{d}\overline{r}^2}-\dfrac{1}{\overline{r}^2}\dfrac{\mathrm{d}W}{\mathrm{d}\overline{r}}+\dfrac{2-\mu}{\overline{r}^2\phi^2}\dfrac{\mathrm{d}^3W}{\mathrm{d}\overline{r}\mathrm{d}\overline{\theta}^2}-\dfrac{3-\mu}{\overline{r}^3\phi^2}\dfrac{\mathrm{d}^2W}{\mathrm{d}\overline{\theta}^2}\right)\right|_{\overline{r}=1}=0\end{cases}\tag{37}$$

3. Discretization Method of Vibration Equation

The differential quadrature method (DQM) is used to solve (34). The DQM [30–32] approximates the derivatives of the function at the given nodes by weighted sums of the function at the total nodes. According to DQM, the annular sector plate adopts the δ method to treat the boundary conditions. The nodes of the plate are calculated by the following formula

$$\begin{aligned}
\overline{r}_1 &= 0,\\
\overline{r}_2 &= \delta,\\
\overline{r}_{N-1} &= 1-\delta,\\
\overline{r}_N &= 1,\\
\overline{r}_i &= \frac{1-\xi}{2}\left(\frac{1+\xi}{1-\xi}+x_i\right) \quad (i=3,\ldots,N-2)\\
\overline{\theta}_1 &= 0,\\
\overline{\theta}_2 &= \delta,\\
\overline{\theta}_{M-1} &= 1-\delta,\\
\overline{\theta}_M &= 1,\\
\overline{\theta}_i &= \frac{1}{2}\left(1-\cos\frac{(j-2)\pi}{M-3}\right) \quad (j=3,\ldots,M-2)
\end{aligned} \tag{38}$$

where $x_i = S_i \in (-1,1)$ $(i = 3,\cdots,N-2)$ is Gauss-Legendre integral point.

Based on the Lagrange interpolation polynomial, the weight coefficients of the first derivative $A_{ij}^{(1)}$ and $B_{km}^{(1)}$ are obtained, respectively.

$$A_{ik}^{(1)} = \begin{cases} \dfrac{\prod_{\substack{\nu=1\\ \nu\neq i,k}}^{N}(\overline{r}_i-\overline{r}_\nu)}{\prod_{\substack{\nu=1\\ \nu\neq k}}^{N}(\overline{r}_k-\overline{r}_\nu)} & (i,k=1,2,\cdots,N;\ k\neq i)\\ \sum\limits_{\substack{\nu=1\\ \nu\neq i}}^{N}\dfrac{1}{\overline{r}_i-\overline{r}_\nu} & (i,k=1,2,\cdots,N;\ k=i) \end{cases} \tag{39}$$

$$B_{jm}^{(1)} = \begin{cases} \dfrac{\prod_{\substack{\nu=1\\ \nu\neq j,m}}^{M}(\overline{\theta}_j-\overline{\theta}_\nu)}{\prod_{\substack{\nu=1\\ \nu\neq m}}^{M}(\overline{\theta}_m-\overline{\theta}_\nu)} & (j,m=1,2,\cdots,M;\ m\neq j)\\ \sum\limits_{\substack{\nu=1\\ \nu\neq j}}^{M}\dfrac{1}{\overline{\theta}_j-\overline{\theta}_\nu} & (j,m=1,2,\cdots,M;\ m=j) \end{cases} \tag{40}$$

In the case of $x = 2,3,...,N-1$ and $y = 2,3,...,M-1$, the weight coefficients of the higher derivatives are as follows.

$$A_{ik}^{(x)} = \begin{cases} x\left(A_{ii}^{(x-1)}A_{ik}^{(1)} - \dfrac{A_{ik}^{(x-1)}}{x_i-x_k}\right) & (i,k=1,2,\cdots,N;\ k\neq i)\\ -\sum\limits_{\substack{\nu=1\\ \nu\neq i}}^{N}A_{i\nu}^{(x)} & (i=1,2,\cdots N;\ 1\le x\le(N-1)) \end{cases} \tag{41}$$

$$B_{jm}^{(y)} = \begin{cases} y\left(B_{jj}^{(y-1)}B_{jm}^{(1)} - \dfrac{B_{jm}^{(y-1)}}{y_j-y_m}\right) & (j,m=1,2,\cdots,M;\ m\neq j)\\ -\sum\limits_{\substack{\nu=1\\ \nu\neq j}}^{M}B_{j\nu}^{(y)} & (j=1,2,\cdots,M;\ 1\le y\le(M-1)) \end{cases} \tag{42}$$

In this paper, $N = M$ is chosen, and (34) can be discretized into the following form by DQM.

$$\begin{aligned}
&(1+\psi)\left(\sum_{k=1}^{N}A_{ik}^{(4)}W_{kj} + \frac{2}{\overline{r}_i}\sum_{k=1}^{N}A_{ik}^{(3)}W_{kj} - \frac{1}{\overline{r}_i^2}\sum_{k=1}^{N}A_{ik}^{(2)}W_{kj}\right.\\
&\quad + \frac{1}{\overline{r}_i^3}\sum_{k=1}^{N}A_{ik}^{(1)}W_{kj} - \frac{2}{\overline{r}_i^3\phi^2}\sum_{k=1}^{N}A_{ik}^{(1)}\sum_{m=1}^{N}B_{jm}^{(2)}W_{km}\\
&\quad \left. + \frac{2}{\overline{r}_i^2\phi^2}\sum_{k=1}^{N}A_{ik}^{(2)}\sum_{m=1}^{N}B_{jm}^{(2)}W_{km} + \frac{4}{\overline{r}_i^4\phi^2}\sum_{m=1}^{N}B_{jm}^{(2)}W_{km}\right.\\
&\quad \left. + \frac{1}{\overline{r}_i^4\phi^4}\sum_{m=1}^{N}B_{jm}^{(4)}W_{km}\right) + \left(-\omega^2W_{ij}\right.\\
&\quad + \frac{2j\omega\eta^{1/2}c}{\phi}\sum_{m=1}^{N}B_{jm}^{(1)}W_{km} + \frac{\eta c^2}{\phi^2}\sum_{m=1}^{N}B_{jm}^{(2)}W_{km}\left.\right)\\
&\quad - \eta\left(N_{1i}\sum_{k=1}^{N}A_{ik}^{(2)}W_{kj} + N_{2i}\frac{1}{\overline{r}_i}\sum_{k=1}^{N}A_{ik}^{(1)}W_{kj}\right.\\
&\quad \left. + N_{2i}\frac{1}{\overline{r}^2\phi^2}\sum_{m=1}^{N}B_{jm}^{(2)}W_{km} - c^2\overline{r}_i\sum_{k=1}^{N}A_{ik}^{(1)}W_k\right) = 0
\end{aligned} \tag{43}$$

The discretization of (35)-(37) can be expressed as follows.

$$\text{CC-CC:}\begin{cases} W_{1j} = W_{Nj} = W_{i1} = W_{iN} = 0, & (i, j = 1, 2, \cdots, N) \\ \sum_{k=1}^{N} A_{ik}^{(1)} W_{kj} = 0, & (i = 2, N-1;\ j = 2, 3, \cdots, N-2) \\ \sum_{m=1}^{N} B_{jm}^{(1)} W_{im} = 0, & (j = 2, N-1;\ i = 2, 3, \cdots, N-2) \end{cases} \tag{44}$$

$$\text{SS-CC:}\begin{cases} W_{1j} = W_{Nj} = W_{i1} = W_{iN} = 0, & (i, j = 1, 2, \cdots, N) \\ \sum_{k=1}^{N} A_{ik}^{(1)} W_{kj} = 0, & (i = 2, N-1;\ j = 2, 3, \cdots, N-2) \\ \frac{1}{\overline{r}_i} \sum_{k=1}^{N} A_{ik}^{(1)} W_{kj} + \frac{1}{\overline{r}_i^2 \phi^2} \sum_{m=1}^{N} B_{jm}^{(2)} W_{im} + \mu \sum_{k=1}^{N} A_{ik}^{(2)} W_{kj} = 0, & (j = 1, N;\ i = 1, 2, \cdots, N) \end{cases} \tag{45}$$

$$\text{SS-FF:}\begin{cases} W_{i1} = W_{iN} = 0, & (i, j = 1, 2, \cdots, N) \\ \frac{1}{\overline{r}_i} \sum_{k=1}^{N} A_{ik}^{(1)} W_{kj} + \frac{1}{\overline{r}_i^2 \phi^2} \sum_{m=1}^{N} B_{jm}^{(2)} W_{im} + \mu \sum_{k=1}^{N} A_{ik}^{(2)} W_{kj} = 0, & (j = 1, N;\ i = 1, 2, \cdots, N) \\ \sum_{k=1}^{N} A_{ik}^{(2)} W_{kj} + \mu \frac{1}{\overline{r}_i} \sum_{k=1}^{N} A_{ik}^{(1)} W_{kj} + \mu \frac{1}{\overline{r}_i^2 \phi^2} \sum_{m=1}^{N} B_{jm}^{(2)} W_{im} = 0, & (i = 1, N;\ j = 1, 2, \cdots, N) \\ \sum_{k=1}^{N} A_{ik}^{(3)} W_{kj} + \frac{1}{\overline{r}_i} \sum_{k=1}^{N} A_{ik}^{(2)} W_{kj} - \frac{1}{\overline{r}_i^2} \sum_{k=1}^{N} A_{ik}^{(1)} W_{kj} + \frac{2-\mu}{\overline{r}_i^2 \phi^2} \sum_{k=1}^{N} A_{ik}^{(1)} \sum_{m=1}^{N} B_{jm}^{(2)} W_{im} - \frac{3-\mu}{\overline{r}_i^3 \phi^2} \sum_{m=1}^{N} B_{jm}^{(2)} W_{im} = 0, & (i = 2, N-1;\ j = 1, 2, \cdots, N) \end{cases} \tag{46}$$

Equation (43) and one of the boundary conditions (44)-(46) can be expressed in the matrix form as

$$\left(\omega^2 [R] + \omega [G] + [K]\right) \left\{W_{kj}\right\} = 0 \tag{47}$$

where the matrices $[R]$, $[G]$, and $[K]$ involve the dimensionless angular speed, the ratio of inner to outer radius, the sector angle, and the dimensionless thermoelastic coupling coefficient. The necessary and sufficient condition when W_{kj} has nonzero solution is that coefficient determinant is equal to zero. Then, the eigenvalue equation of the thermoelastic coupling vibration of rotating annular sector plate is as follows.

$$\left|\omega^2 [R] + \omega [G] + [K]\right| = 0 \tag{48}$$

In (48), ω is a complex eigenvalue. Therefore, one can obtain the complex frequency of the annular sector plate with various parameter values by solving the eigenvalue equation.

4. Numerical Results and Discussion

When $\psi = 0$ and $c = 0$, (34) can be reduced to the differential equation of transverse vibration of the nonrotating annular sector plate. The first five order natural frequencies of the nonrotating annular sector plate with three different boundary conditions are calculated in the case of $\xi = 0.5$ and $\mu = 0.3$. The frequency parameter in this study is defined by $\omega_D = (b^2\omega/h)\sqrt{12\rho(1-\mu^2)/E}$, while the frequency parameter in [14, 33, 34] is defined by $\omega_R = ((b-a)^2\omega/h)\sqrt{12\rho(1-\mu^2)/E}$. When $\xi = a/b = 0.5$, $\omega_D = 4\omega_R$. The calculation results by conversing ω_D to ω_R are in good agreement with those exhibited in [14, 33, 34], which can be seen in Table 1, where the node number is $N = 11$.

4.1. Rotating Annular Sector Plate with CC-CC. Figure 3 shows the variation of the first three order dimensionless complex frequencies of the rotating annular sector plate ($\phi = \pi/3$, $\xi = 0.5$) with the dimensionless angular speed for the dimensionless thermoelastic coupling coefficient $\psi = 0$. When the dimensionless angular speed $c = 0$, the first three order dimensionless complex frequencies ω are real numbers. With the increase of the dimensionless angular speed, the real parts $\mathrm{Re}(\omega)$ of the first three order dimensionless complex frequencies decrease, while their imaginary parts $\mathrm{Im}(\omega)$ remain zero. When the dimensionless angular speed reaches a certain critical speed $c = 7.34$, the real part of the first order dimensionless complex frequency becomes zero, while its imaginary part has two branches. The critical speed $c_d = 7.34$ is called the first order critical divergence speed. The divergence instability appears in the first order mode of the rotating annular sector plate in the region of $7.34 \le c \le 7.55$. When $7.55 < c \le 8.11$, the rotating annular sector plate regains stability, and subsequently in the case of $8.11 < c \le 8.61$, the real parts of the first and second order complex frequencies merge with each other and keep positive, while their imaginary parts become two branches with positive and

Table 1: First five order dimensionless natural frequencies of the non-rotating annular sector plate ($\xi = 0.5$, $\mu = 0.3$).

Sector angle	Boundary condition	Methods	ω_1	ω_2	ω_3	ω_4	ω_5
$\pi/6$	SS-CC	Reference[14] (ω_R)	33.90	75.11	76.46	121.8	135.3
		Present ($\omega = \omega_D/4$)	33.9230	75.1841	76.4747	121.9212	135.2661
	CC-CC	Reference[14] (ω_R)	48.04	85.52	104.4	142.8	151.3
		Present ($\omega = \omega_D/4$)	48.1164	85.6430	104.5898	142.7932	151.5388
	SS-FF	Reference[14] (ω_R)	11.70	28.87	44.03	50.51	82.13
		Present ($\omega = \omega_D/4$)	11.7792	28.8884	44.0803	50.5733	82.1813
$\pi/4$	SS-CC	Reference[14] (ω_R)	26.89	44.70	67.37	76.45	86.60
		Reference[33] (ω_R)	26.91	44.69	74.03	77.34	88.32
		Present ($\omega = \omega_D/4$)	26.9225	44.7239	67.4507	76.4300	86.6895
	CC-CC	Reference[14] (ω_R)	31.39	56.85	70.22	94.54	96.73
		Present ($\omega = \omega_D/4$)	31.4375	56.9450	70.3175	94.3425	96.8775
	SS-FF	Reference[14] (ω_R)	5.267	16.68	20.40	36.60	44.03
		Present ($\omega = \omega_D/4$)	5.2730	16.6916	20.4240	36.6488	44.0779
$\pi/3$	SS-CC	Reference[14] (ω_R)	24.74	33.89	51.44	64.79	75.08
		Present ($\omega = \omega_D/4$)	24.7623	33.9237	51.4538	64.8695	75.1838
	CC-CC	Reference[14] (ω_R)	26.53	39.85	61.49	65.96	79.38
		Present ($\omega = \omega_D/4$)	26.5729	39.9165	61.4045	66.0465	79.5028
	SS-FF	Reference[14] (ω_R)	2.856	11.77	11.87	25.51	28.87
		Present ($\omega = \omega_D/4$)	2.8601	11.7788	11.8736	25.5408	28.8883
$\pi/2$	SS-CC	Reference[14] (ω_R)	23.33	26.88	33.87	44.65	58.96
		Present ($\omega = \omega_D/4$)	23.3613	26.9207	33.9137	45.3747	56.4011
	CC-CC	Reference[14] (ω_R)	23.80	28.73	37.63	50.33	63.30
		Reference[34] (ω_R)	23.83	28.77	37.69	50.42	63.30
		Present ($\omega = \omega_D/4$)	23.8389	28.7775	37.6349	50.4611	63.2698
	SS-FF	Reference[14] (ω_R)	1.068	5.267	7.779	11.77	16.68
		Present ($\omega = \omega_D/4$)	1.0697	5.2728	7.7841	11.7778	16.6914

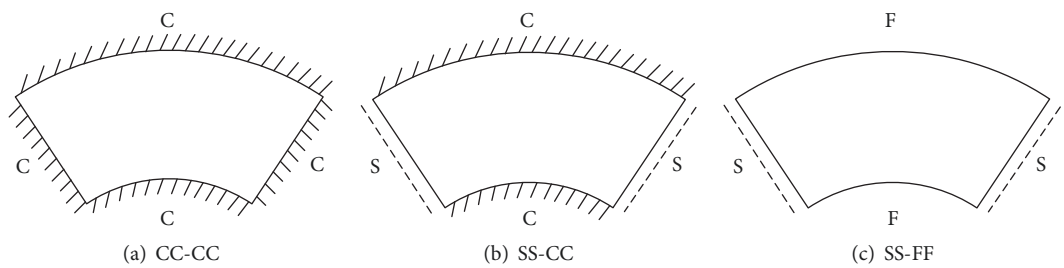

(a) CC-CC (b) SS-CC (c) SS-FF

Figure 2: Definitions of the boundary conditions.

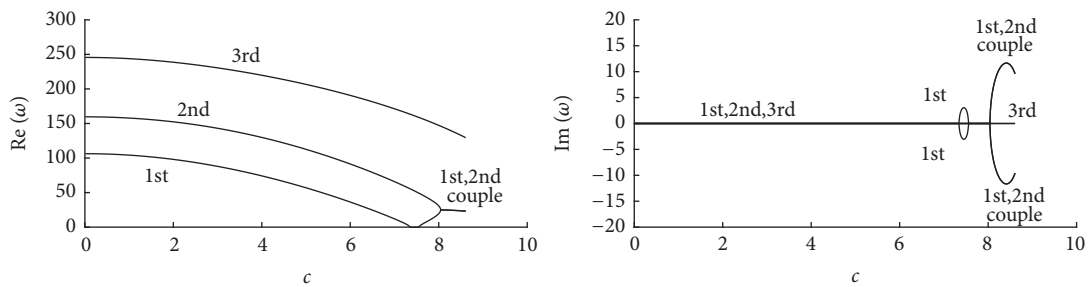

Figure 3: First three order dimensionless complex frequencies versus dimensionless angular speed ($\phi = \pi/3$, $\xi = 0.5$, $\psi = 0$).

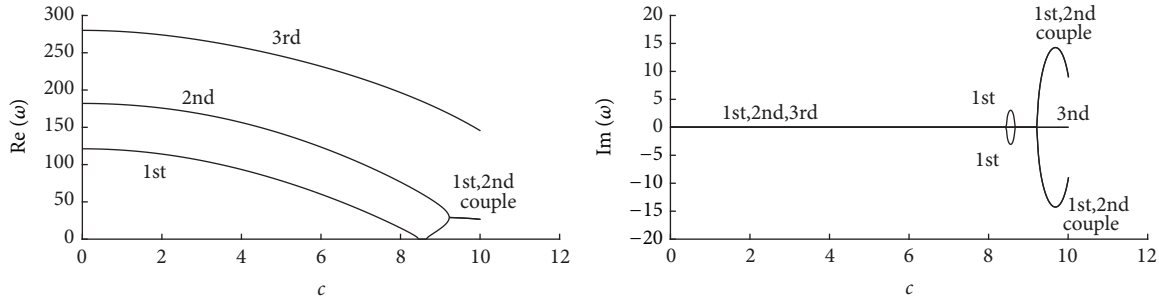

Figure 4: First three order dimensionless complex frequencies versus dimensionless angular speed ($\phi = \pi/3$, $\xi = 0.5$, $\psi = 0.3$).

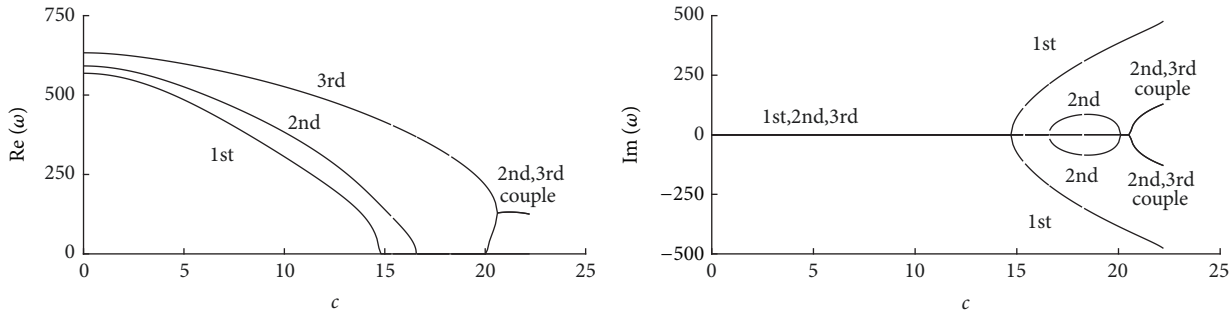

Figure 5: First three order dimensionless complex frequencies versus dimensionless angular speed ($\phi = \pi/3$, $\xi = 0.8$, $\psi = 0$).

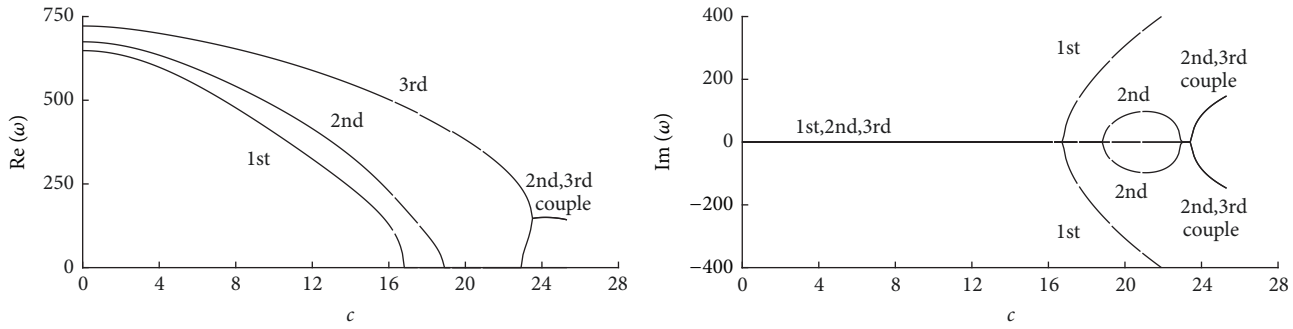

Figure 6: First three order dimensionless complex frequencies versus dimensionless angular speed ($\phi = \pi/3$, $\xi = 0.8$, $\psi = 0.3$).

negative values. The result shows that the annular sector plate undergoes a coupled-mode flutter instability of the first and second order modes. $c_f = 8.11$ is called the first-second order critical flutter speed.

Figure 4 shows the variation of the first three order dimensionless complex frequencies of the rotating annular sector plate ($\phi = \pi/3$, $\xi = 0.5$) with the dimensionless angular speed c for the dimensionless thermoelastic coupling coefficient $\psi = 0.3$. In the case of thermoelastic coupling ($\psi = 0.3$), the real parts of the first three order dimensionless complex frequencies at $c = 0$ are greater than those in the case of uncoupling ($\psi = 0$), and the annular sector plate undergoes the divergence instability in the first order mode and the coupled-mode flutter instability of the first and second order modes. The first order critical divergence speed and the first-second order critical flutter speed in the case of thermoelastic coupling are $c_d = 8.45$ and $c_f = 9.23$, respectively, which are greater than those in the case of uncoupling.

Figures 5 and 6 show the variation of the first three order dimensionless complex frequencies ω of the rotating annular sector plate ($\phi = \pi/3$, $\xi = 0.8$) with the dimensionless angular speed for $\psi = 0$ and $\psi = 0.3$. In comparison with Figures 3 and 4, we can see that when the ratio of inner to outer radius increases from 0.5 to 0.8, the real parts of the first three order dimensionless complex frequencies increase at the dimensionless angular speed $c = 0$. With the increase of c, the real parts of ω in the first and second modes become zero successively, and then the imaginary parts of ω have two branches with positive and negative values. This shows that the annular sector plate undergoes the divergence instability of the first and second modes, and the corresponding first order critical divergence speed increases with the increase of the ratio of inner to outer radius. When the dimensionless angular speed further increases, the annular sector plate undergoes the coupled-mode flutter instability of the second and third order modes. By comparing Figure 5 with Figure 6, it is found that the corresponding critical speed in the

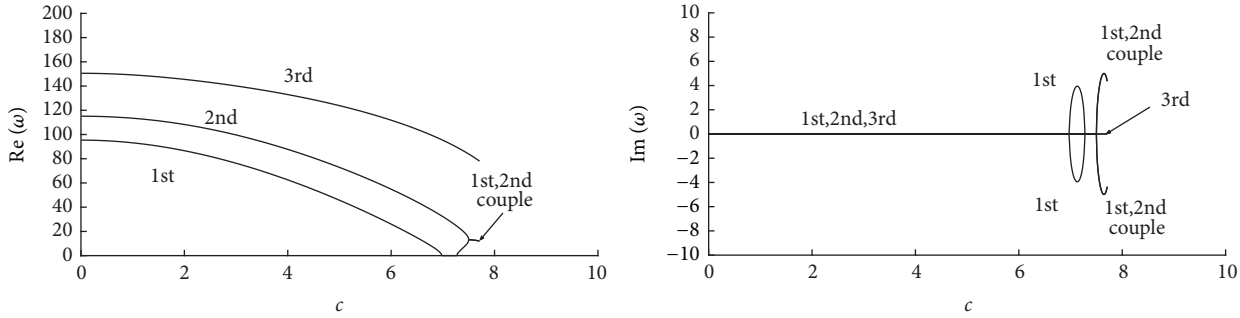

Figure 7: First three order dimensionless complex frequencies versus dimensionless angular speed ($\phi = \pi/2$, $\xi = 0.5$, $\psi = 0$).

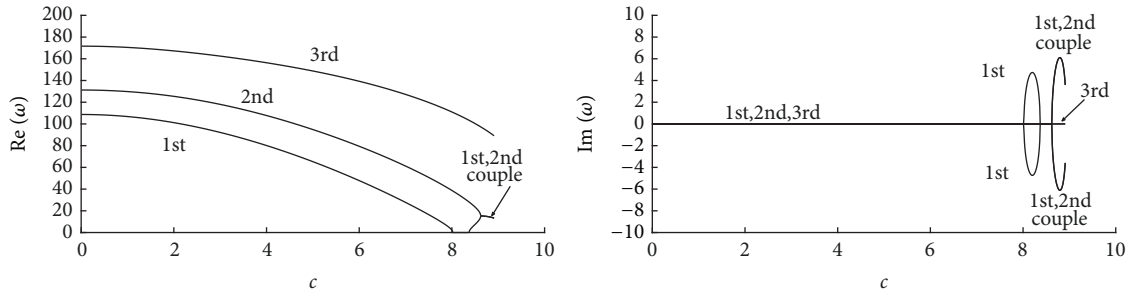

Figure 8: First three order dimensionless complex frequencies versus dimensionless angular speed ($\phi = \pi/2$, $\xi = 0.5$, $\psi = 0.3$).

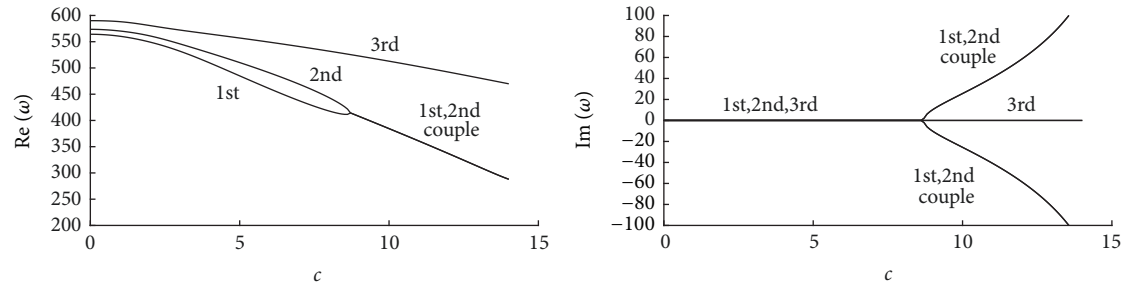

Figure 9: First three order dimensionless complex frequencies versus dimensionless angular speed ($\phi = \pi/2$, $\xi = 0.8$, $\psi = 0$).

thermoelastic coupling case is greater than that in the case of uncoupling.

Figures 7 and 8 show the variation of the first three order dimensionless complex frequencies of the rotating annular sector plate ($\phi = \pi/2$, $\xi = 0.5$) with the dimensionless angular speed for $\psi = 0$ and $\psi = 0.3$. The annular sector plate undergoes the divergence instability in the first order mode and the coupled-mode flutter instability of the first and second order modes, and the first order critical divergence speed and the first-second order critical flutter speed increase when the dimensionless thermoelastic coupling coefficient increases from 0 to 0.3. From Figures 3, 4, 7, and 8, it is obtained that when other parameters are invariable, the real parts of the first three order dimensionless complex frequencies at $c = 0$, the first order critical divergence speed, and the first-second order critical flutter speed decrease with the increase of the sector angle ϕ.

Figures 9 and 10 show the variation of the first three order dimensionless complex frequencies of the rotating annular sector plate ($\phi = \pi/2, \xi = 0.8$) with the dimensionless angular speed for $\psi = 0$ and $\psi = 0.3$. In comparison with Figures 7 and 8, it is observed that when the ratio of inner to outer radius increases from 0.5 to 0.8, the divergence instability of the first order mode does not occur, while the coupled-mode flutter instability of the first and second order modes appears, and the corresponding first-second order critical flutter speed increases with the increase of the ratio of inner to outer radius. By comparing Figure 9 with Figure 10, it can be seen that the first-second order critical flutter speed increases with the increase of the dimensionless thermoelastic coupling coefficient when other parameters are invariable.

From Figures 3–10, one can see that when the sector angle increases from $\pi/3$ to $\pi/2$, the type of instability does not change in the case of the ratio of inner to outer radius $\xi = 0.5$, while it changes in the case of $\xi = 0.8$.

4.2. Rotating Annular Sector Plate with SS-CC. Figures 11 and 12 show the variation of the first three order dimensionless complex frequencies of the rotating annular sector plate ($\phi = \pi/3$, $\xi = 0.5$) with the dimensionless angular speed for the

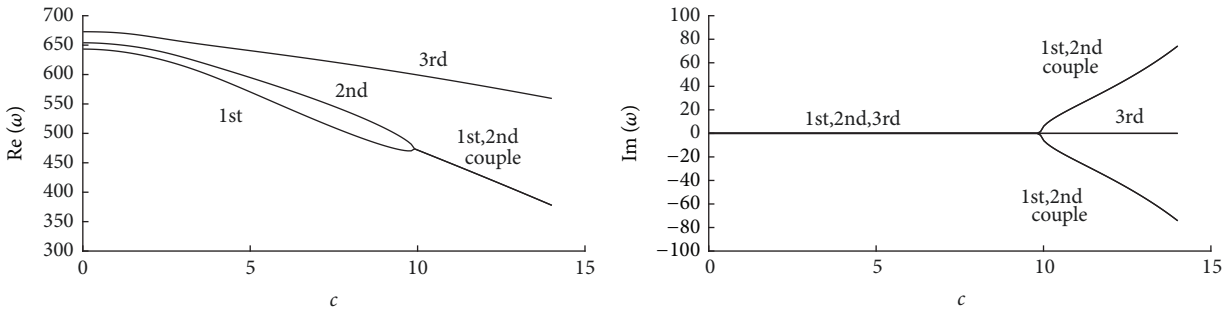

Figure 10: First three order dimensionless complex frequencies versus dimensionless angular speed ($\phi = \pi/2$, $\xi = 0.8$, $\psi = 0.3$).

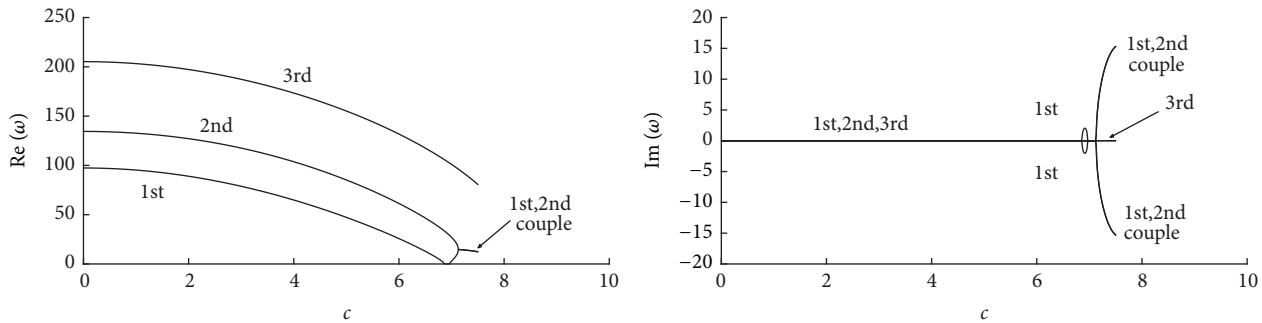

Figure 11: First three order dimensionless complex frequencies versus dimensionless angular speed ($\phi = \pi/3$, $\xi = 0.5$, $\psi = 0$).

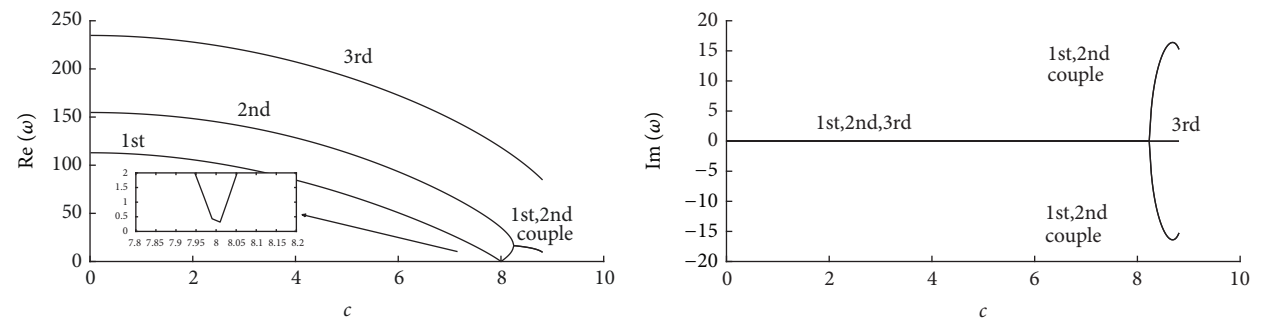

Figure 12: First three order dimensionless complex frequencies versus dimensionless angular speed ($\phi = \pi/3$, $\xi = 0.5$, $\psi = 0.3$).

dimensionless thermoelastic coupling coefficient $\psi = 0$ and $\psi = 0.3$. As can be seen from Figure 11, the plate undergoes the divergence instability of the first order mode and the coupled-mode flutter instability of the first and second order modes in the case of thermoelastic uncoupling. However, for $\psi = 0.3$, with the increase of c, the real part of the first order dimensionless complex frequency remains a positive value, which decreases firstly and then increases. The annular sector plate does not undergo the divergence instability of the first order mode while it only undergoes the coupled-mode flutter instability of the first and second order modes. It shows that the dimensionless thermoelastic coupling coefficient can change the type of instability of the annular sector plate. By comparing Figure 11 with Figure 12, it is found that when $c = 0$, the real parts of the first three order dimensionless complex frequencies in the thermoelastic coupling case are greater than that in the case of uncoupling.

Figures 13 and 14 show the variation of the first three order dimensionless complex frequencies of the rotating annular sector plate ($\phi = \pi/3, \xi = 0.8$) with the dimensionless angular speed for $\psi = 0$ and $\psi = 0.3$. The values of the real parts of the second and third order dimensionless complex frequencies of the annular sector plate present declining, rising, and declining tendency. The annular sector plate undergoes the divergence instability of the first order mode and the coupled-mode flutter instability of the first and second order modes, and the corresponding critical speed in the thermoelastic coupling case is greater than that in the case of uncoupling.

Figures 15 and 16 show the variation of the first three order dimensionless complex frequencies of the rotating annular sector plate ($\phi = \pi/2$, $\xi = 0.5$) with the dimensionless angular speed for $\psi = 0$ and $\psi = 0.3$. we can see that the annular sector plate undergoes the divergence instability of the first order mode firstly, then it undergoes the coupled-mode flutter instability of the first and second

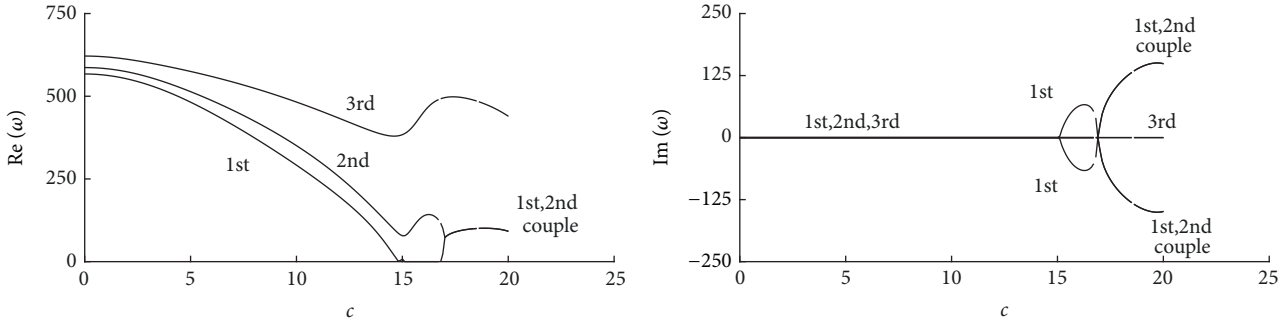

Figure 13: First three order dimensionless complex frequencies versus dimensionless angular speed ($\phi = \pi/3$, $\xi = 0.8$, $\psi = 0$).

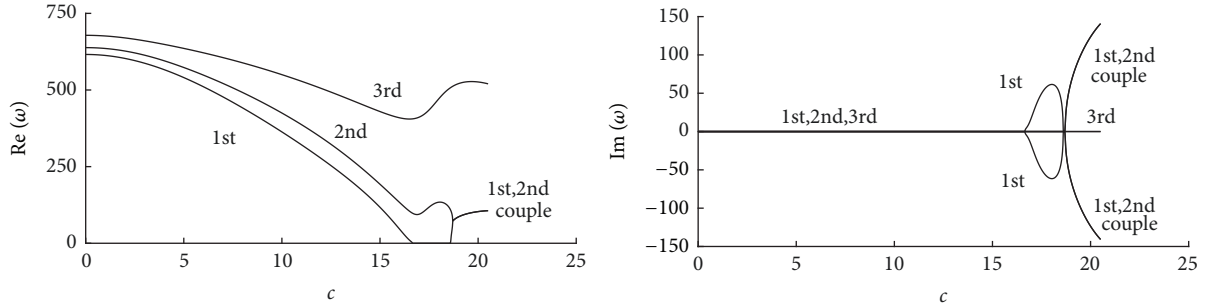

Figure 14: First three order dimensionless complex frequencies versus dimensionless angular speed ($\phi = \pi/3$, $\xi = 0.8$, $\psi = 0.3$).

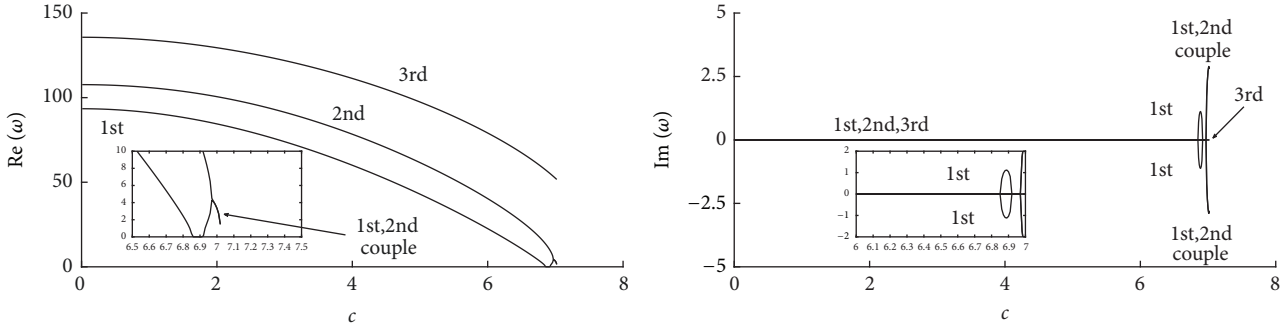

Figure 15: First three order dimensionless complex frequencies versus dimensionless angular speed ($\phi = \pi/2$, $\xi = 0.5$, $\psi = 0$).

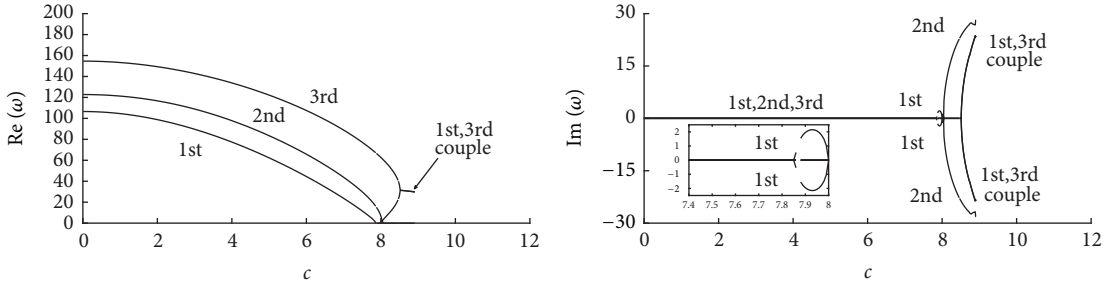

Figure 16: First three order dimensionless complex frequencies versus dimensionless angular speed ($\phi = \pi/2$, $\xi = 0.5$, $\psi = 0.3$).

order modes in the thermoelastic uncoupling case. However, it undergoes the divergence instability of the first and second order mode and the coupled-mode flutter instability of the first and third order modes in the thermoelastic coupling case.

Figures 17 and 18 show the variation of the first three order dimensionless complex frequencies of the rotating annular sector plate ($\phi = \pi/2, \xi = 0.8$) with the dimensionless angular speed for $\psi = 0$ and $\psi = 0.3$. In the case of $\xi = 0.8$, the annular sector plate only undergoes the coupled-mode

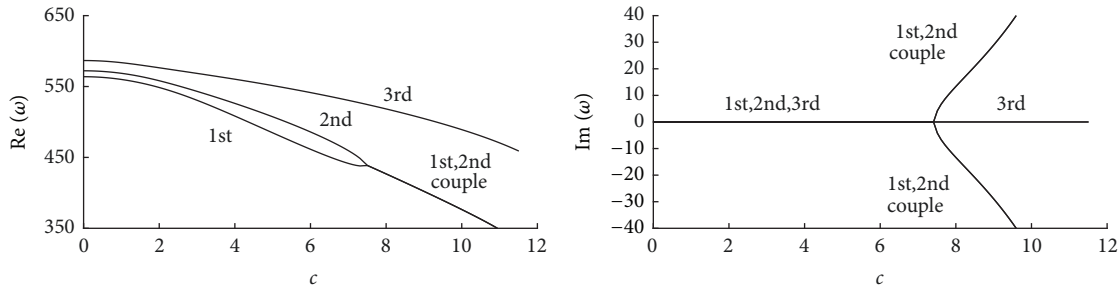

Figure 17: First three order dimensionless complex frequencies versus dimensionless angular speed ($\phi = \pi/2$, $\xi = 0.8$, $\psi = 0$).

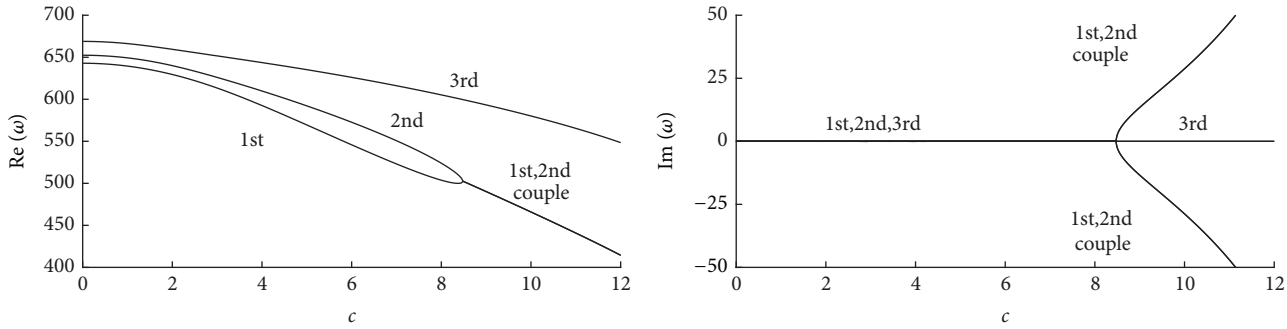

Figure 18: First three order dimensionless complex frequencies versus dimensionless angular speed ($\phi = \pi/2$, $\xi = 0.8$, $\psi = 0.3$).

flutter instability in the first and second order modes. The corresponding first-second order critical flutter speed in the thermoelastic coupling case is greater than that in the case of uncoupling.

4.3. Rotating Annular Sector Plate with SS-FF. Figures 19–22 show the variation of the first three order dimensionless complex frequencies of the rotating annular sector plate ($\phi = \pi/3$, $\phi = \pi/2$, $\xi = 0.5$) with the dimensionless angular speed for the dimensionless thermoelastic coupling coefficient $\psi = 0$ and $\psi = 0.3$. We can see that rotating annular sector plate with SS-FF undergoes the divergence instability in the first order mode and the coupled-mode flutter instability of the first and second order modes. The corresponding critical speed in the thermoelastic coupling case is greater than that in the case of uncoupling. When the ratio of inner to outer radius $\xi = 0.5$, the corresponding critical speed deceases with the increase of the sector angle.

Figures 23–26 show the variation of the first three order dimensionless complex frequencies of the rotating annular sector plate ($\phi = \pi/3$, $\phi = \pi/2$, $\xi = 0.8$) with the dimensionless angular speed for the dimensionless thermoelastic coupling coefficient $\psi = 0$ and $\psi = 0.3$. Compared with the case of $\xi = 0.5$, besides the divergence instability in the first order mode and the coupled-mode flutter instability of the first and second order modes, the rotating annular sector plate with SS-FF also undergoes the divergence instability in the second order mode. When other parameters are invariable, the corresponding critical speed deceases with the increase of the sector angle, but increases with the increase of the dimensionless thermoelastic coupling coefficient.

From Figures 19–26, we can see that if the sector angle and dimensionless thermoelastic coupling coefficient are constant, when the ratio of inner to outer radius increases from $\xi = 0.5$ to $\xi = 0.8$, the first order critical divergence speed decreases, while the first-second order critical flutter speed increases.

5. Conclusions

The thermoelastic coupling transverse vibration and stability of the rotating annular sector plate with three boundaries are investigated by DQM. The effects of the dimensionless angular speed, the ratio of inner to outer radius, the sector angle, the dimensionless thermoelastic coupling coefficient, and the boundary condition on transverse vibration and stability are discussed. The results are listed as follows.

(1) When other parameters are invariable, the real parts of the first three order dimensionless complex frequencies of the nonrotating annular sector plate ($c = 0$) decrease with the increase of the sector angle. And their values in the case of thermoelastic coupling are greater than that in the case of uncoupling.

(2) The increase of the dimensionless thermoelastic coupling coefficient can change the type of instability of the annular sector plate under CC-CC and SS-CC boundary conditions, but it does not change under SS-FF boundary

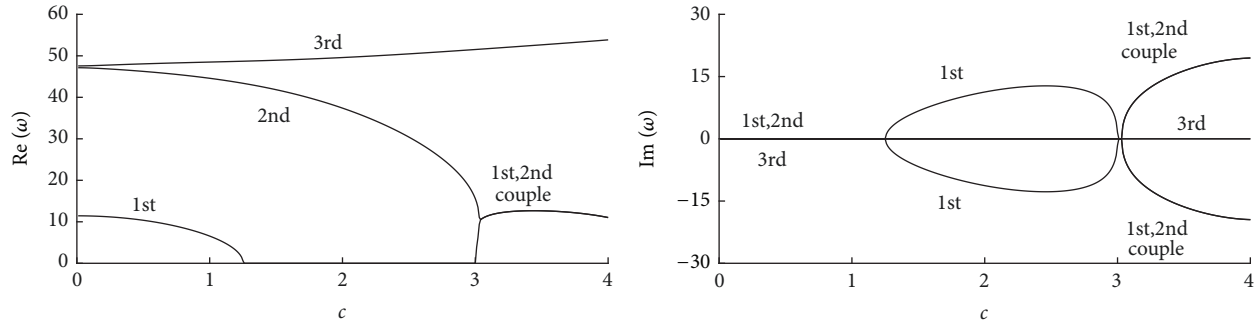

Figure 19: First three order dimensionless complex frequencies versus dimensionless angular speed ($\phi = \pi/3$, $\xi = 0.5$, $\psi = 0$).

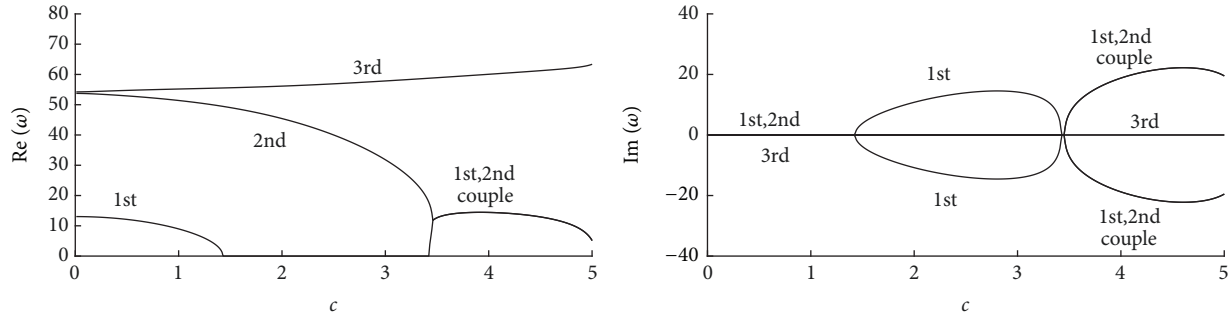

Figure 20: First three order dimensionless complex frequencies versus dimensionless angular speed ($\phi = \pi/3$, $\xi = 0.5$, $\psi = 0.3$).

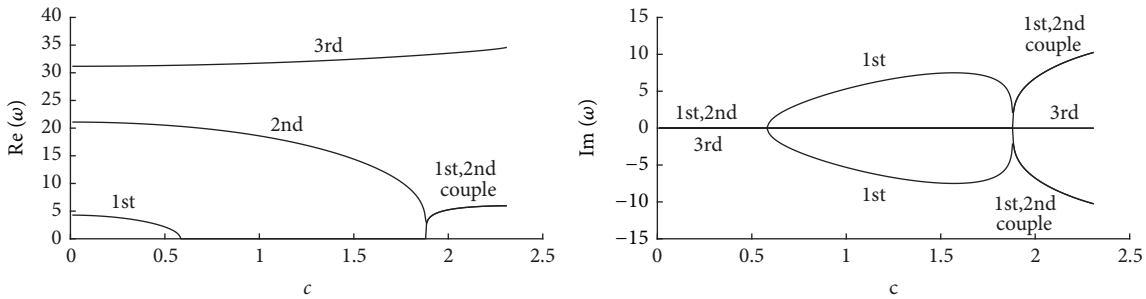

Figure 21: First three order dimensionless complex frequencies versus dimensionless angular speed ($\phi = \pi/2$, $\xi = 0.5$, $\psi = 0$).

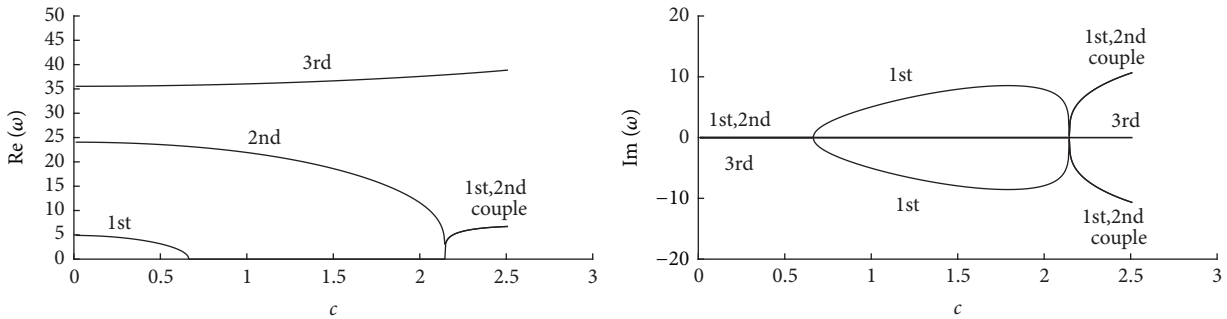

Figure 22: First three order dimensionless complex frequencies versus dimensionless angular speed ($\phi = \pi/2$, $\xi = 0.5$, $\psi = 0.3$).

condition. The corresponding critical speed in the case of thermoelastic coupling is greater than that in the case of uncoupling when other parameters and the type of instability are invariable.

(3) The annular sector plate undergoes the divergence instability and the coupled-mode flutter instability under the three boundary conditions; however, the modes undergoing these two kinds of instability are different, which depend on the ratio of inner to outer radius, the sector angle, the dimensionless thermoelastic coupling coefficient, and the boundary condition.

Data Availability

The data used to support the findings of this study are available from the corresponding author upon request.

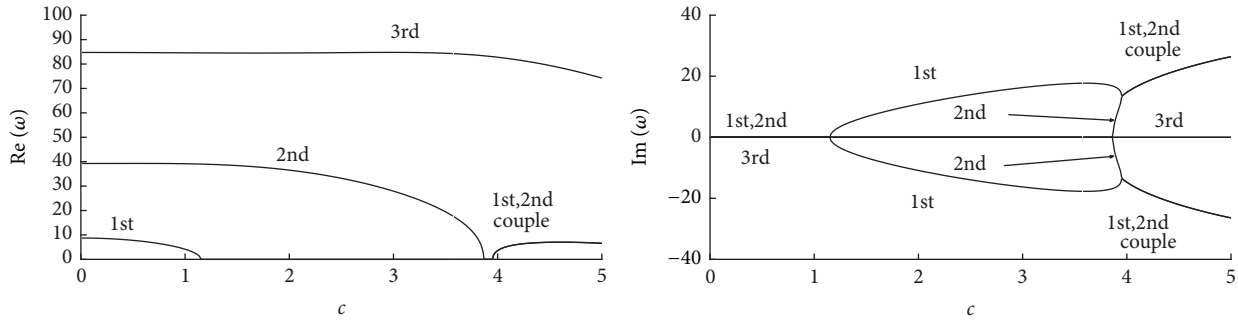

Figure 23: First three order dimensionless complex frequencies versus dimensionless angular speed ($\phi = \pi/3$, $\xi = 0.8$, $\psi = 0$).

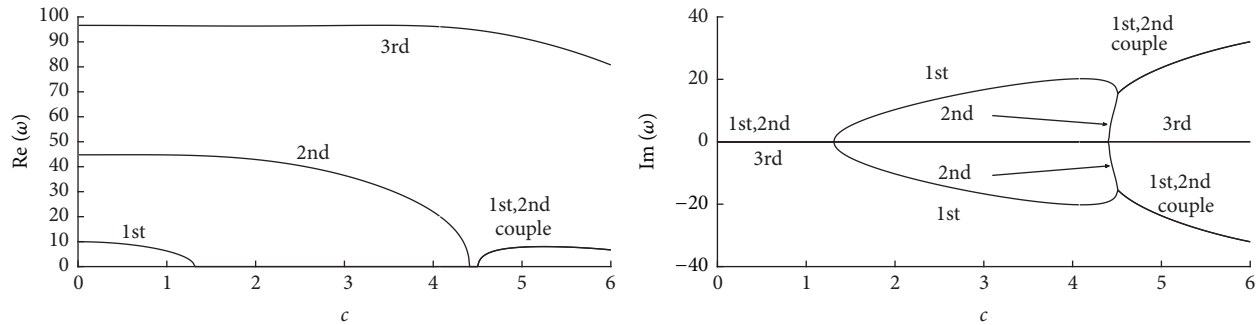

Figure 24: First three order dimensionless complex frequencies versus dimensionless angular speed ($\phi = \pi/3$, $\xi = 0.8$, $\psi = 0.3$).

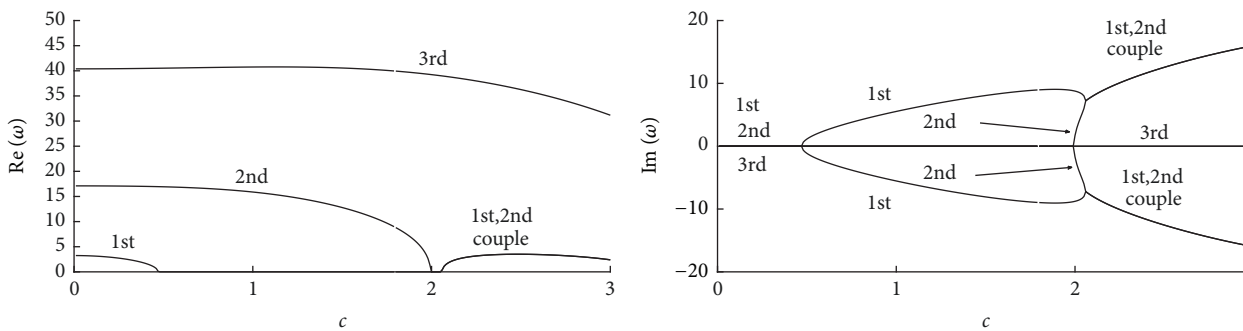

Figure 25: First three order dimensionless complex frequencies versus dimensionless angular speed ($\phi = \pi/2$, $\xi = 0.8$, $\psi = 0$).

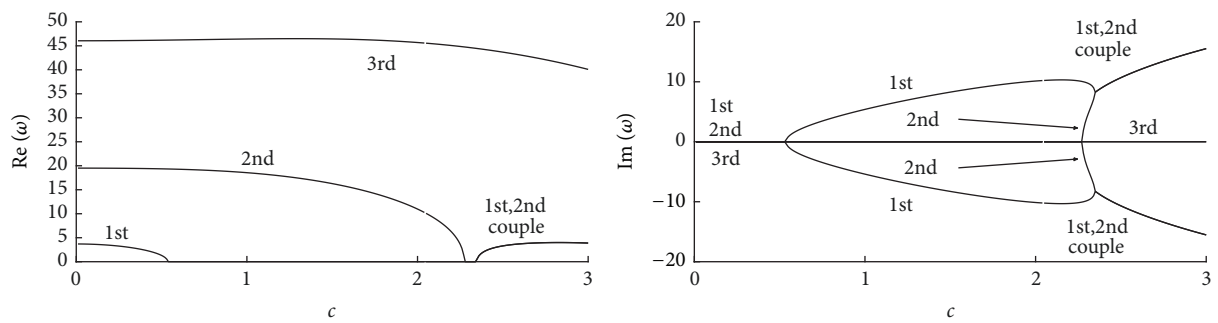

Figure 26: First three order dimensionless complex frequencies versus dimensionless angular speed ($\phi = \pi/2$, $\xi = 0.8$, $\psi = 0.3$).

Conflicts of Interest

The authors declare that there are no conflicts of interest regarding the publication of this paper.

Acknowledgments

The authors gratefully acknowledge the support of the National Natural Science Foundation of China (No. 11472211).

References

[1] E. Jomehzadeh, A. R. Saidi, and S. R. Atashipour, "An analytical approach for stress analysis of functionally graded annular sector plates," *Materials and Corrosion*, vol. 30, no. 9, pp. 3679–3685, 2009.

[2] S. Sahraee, "Bending analysis of functionally graded sectorial plates using Levinson plate theory," *Composite Structures*, vol. 88, no. 4, pp. 548–557, 2009.

[3] F. Fallah and A. Nosier, "Thermo-mechanical behavior of functionally graded circular sector plates," *Acta Mechanica*, vol. 226, no. 1, pp. 37–54, 2015.

[4] M. G. Qian and Z. D. Yan, "Solution of sector plate by Fourier-Bessel series," *Applied Mathematics and Mechnics*, vol. 6, no. 4, pp. 359–376, 1985.

[5] X. J. Shi, D. Y. Shi, W. L. Li, and Q. S. Wang, "A unified method for free vibration analysis of circular, annular and sector plates with arbitrary boundary conditions," *Journal of Vibration and Control*, vol. 22, no. 2, pp. 442–456, 2016.

[6] D. Y. Shi, X. J. Shi, W. L. Li, Q. S. Wang, and J. S. Han, "Vibration analysis of annular sector plates under different boundary conditions," *Shock and Vibration*, vol. 2014, Article ID 517946, 11 pages, 2014.

[7] Q. S. Wang, D. Y. Shi, Q. Liang, and F. E. Ahad, "A unified solution for free in-plane vibration of orthotropic circular, annular and sector plates with general boundary conditions," *Applied Mathematical Modelling*, vol. 40, no. 21, pp. 9228–9253, 2016.

[8] R. Zhong, Q. S. Wang, J. Y. Tang, C. J. Shuai, and B. Qin, "Vibration analysis of functionally graded carbon nanotube reinforced composites (FG-CNTRC) circular, annular and sector plates," *Composite Structures*, vol. 194, pp. 49–67, 2018.

[9] X. L. Guan, J. Y. Tang, D. Y. Shi, C. J. Shuai, and Q. S. Wang, "A semi-analytical method for transverse vibration of sector-like thin plate with simply supported radial edges," *Applied Mathematical Modelling: Simulation and Computation for Engineering and Environmental Systems*, vol. 60, no. 3, pp. 48–63, 2018.

[10] D. Zhao, F. Xie, A. L. Wang, C. J. Shuai, J. Y. Tang, and Q. S. Wang, "Dynamics analysis of functionally graded porous (FGP) circular, annular and sector plates with general elastic restraints," *Composites Part B: Engineering*, vol. 159, pp. 20–43, 2019.

[11] A. S. Rezaei and A. R. Saidi, "An analytical study on the free vibration of moderately thick fluid-infiltrated porous annular sector plates," *Journal of Vibration and Control*, vol. 24, no. 18, pp. 4130–4144, 2018.

[12] D. Zhou, S. H. Lo, and Y. K. Cheung, "3-D vibration analysis of annular sector plates using the Chebyshev-Ritz method," *Journal of Sound and Vibration*, vol. 320, no. 1-2, pp. 421–437, 2009.

[13] S. A. Belalia and A. Houmat, "Nonlinear free vibration of functionally graded shear deformable sector plates by a curved triangular p-element," *European Journal of Mechanics - A/Solids*, vol. 35, pp. 1–9, 2012.

[14] T. Mizusawa, "Application of the spline element method to analyze vibration of annular sector plates," *Journal of Sound and Vibration*, vol. 149, no. 3, pp. 461–470, 1991.

[15] H. Behzad, A. Shaterzadeh, and M. Shariyat, "Thermal buckling analysis of functionally graded perforated annular sector plates using 3D elasticity theory," *Journal of Thermal Stresses*, vol. 40, no. 12, pp. 1–8, 2017.

[16] A. Shaterzadeh, H. Behzad, and M. Shariyat, "Stability analysis of composite perforated annular sector plates under thermo-mechanical loading by finite element method," *International Journal of Structural Stability and Dynamics*, vol. 18, no. 7, Article ID 1850100, p. 23, 2018.

[17] S. H. Mirtalaie, "Differential quadrature free vibration analysis of functionally graded thin annular sector plates in thermal environments," *Journal of Dynamic Systems, Measurement, and Control*, vol. 140, no. 10, 2018.

[18] R. M. H. Khorasany and S. G. Hutton, "An analytical study on the effect of rigid body translational degree of freedom on the vibration characteristics of elastically constrained rotating disks," *International Journal of Mechanical Sciences*, vol. 52, no. 9, pp. 1186–1192, 2010.

[19] H. F. Bauer and W. Eidel, "Transverse vibration and stability of spinning circular plates of constant thickness and different boundary conditions," *Journal of Sound and Vibration*, vol. 300, no. 3-5, pp. 877–895, 2007.

[20] Y. Wang, Z. Tian, J. M. Wu, X. X. Guo, and M. Y. Shao, "Dynamic stability of an axially moving paper board with added subsystems," *Journal of Low Frequency Noise, Vibration and Active Control*, vol. 37, no. 1, pp. 48–59, 2018.

[21] R. Bellman and J. Casti, "Differential quadrature and long-term integration," *Journal of Mathematical Analysis and Applications*, vol. 34, no. 2, pp. 235–238, 1971.

[22] A. G. Striz, W. L. Chen, and C. W. Bert, "Free vibration of plates by the high accuracy quadrature element method," *Journal of Sound and Vibration*, vol. 202, no. 2, pp. 51–62, 1997.

[23] G. Karamia, P. Malekzadehb, and S. R. Mohebpourb, "DQM free vibration analysis of moderately thick symmetric laminated plates with elastically restrained edges," *Composite Structures*, vol. 74, no. 1, pp. 115–125, 2006.

[24] T. Y. Wu, Y. Y. Wang, and G. R. Liu, "Free vibration analysis of circular plates using generalized differential quadrature rule," *Computer Methods Applied Mechanics and Engineering*, vol. 191, no. 46, pp. 5365–5380, 2002.

[25] P. Malekzadeh and S. A. Shahpari, "Free vibration analysis of variable thickness thin and moderately thick plates with elastically restrained edges by DQM," *Thin-Walled Structures*, vol. 43, no. 7, pp. 1037–1050, 2005.

[26] F. Tornabene, E. Viola, and D. J. Inman, "2-D differential quadrature solution for vibration analysis of functionally graded conical, cylindrical shell and annular plate structures," *Journal of Sound and Vibration*, vol. 328, no. 3, pp. 259–290, 2009.

[27] F. Tornabene, "Free vibration analysis of functionally graded conical, cylindrical shell and annular plate structures with a four-parameter power-law distribution," *Computer Methods*

Applied Mechanics and Engineering, vol. 198, no. 37-40, pp. 2911–2935, 2009.

[28] N. Fantuzzi, F. Tornabene, M. Bacciocchi, and R. Dimitri, "Free vibration analysis of arbitrarily shaped functionally graded carbon nanotube-reinforced plates," *Composites Part B: Engineering*, vol. 115, pp. 384–408, 2017.

[29] M. H. Shao, J. M. Wu, Y. Wang, Q. M. Wu, and Y. Chen, "Vibration characteristics for moving printing membrane with variable density along the lateral direction," *Shock and Vibration*, vol. 2017, Article ID 2968705, 10 pages, 2017.

[30] A. Alibeigloo and A. Emtehani, "Static and free vibration analyses of carbon nanotube-reinforced composite plate using differential quadrature method," *Meccanica*, vol. 50, no. 1, pp. 61–76, 2015.

[31] J.-B. Han and K. M. Liew, "Analysis of moderately thick circular plates using differential quadrature method," *Journal of Engineering Mechanics*, vol. 123, no. 12, pp. 1247–1252, 1997.

[32] C. Shu and W. Chen, "On optimal selection of interior points for applying discretized boundary conditions in DQ vibration analysis of beams and plates," *Journal of Sound and Vibration*, vol. 222, no. 2, pp. 239–257, 1999.

[33] R. Ramakrishnan and V. X. Kunukkasseril, "Free vibration of stiffened circular bridge decks," *Journal of Sound and Vibration*, vol. 44, no. 2, pp. 209–221, 1976.

[34] G. N. Geannakakes, "Vibration analysis of arbitrarily shaped plates using beam characteristic orthogonal polynomials in the semi-analytical finite strip method," *Journal of Sound and Vibration*, vol. 137, no. 2, pp. 283–303, 1990.